AN ABSTRACT OF THE THESIS OF

Bi-De Qin for the degree of Master of Science in Electrical Engineering presented on December 8, 1988

Title: Operating Characteristics of the Brushless Doubly Fed Machine

Redacted for privacy

Abstract approved:

Hian K. Lauw

The brushless doubly fed machine (BDFM), or self-cascade single-frame machine, can operate asynchronously or synchronously over a wide speed range. In this sense the machine becomes an adjustable speed synchronous machine. Such machines may become unstable in certain regions of operation. Analyzing its steady-state performance and determining its stable operating regions are very important efforts to pursue. This thesis presents the theory and its verification in order to predict the steady-state operating performance of the BDFM using a method based on circle diagrams. The stable regions and the loci of operating points for different mechanical input characteristics are presented.

Operating Characteristics of the Brushless Doubly Fed Machine

by

Bi-De Qin

A THESIS

submitted to

Oregon State University

in partial fulfillment of

the requirements for the

degree of

Master of Science

Completed December 8, 1988

Commencement June 1989

APPROVED:

Redacted for privacy

Associate Professor of Electrical and Computer Engineering in charge of major

Redacted for privacy

Head of Department of Electrical and Computer Engineering

Redacted for privacy

Dean of Graduate School

Date thesis is presented December 8, 1988

Typed by Bi-De Qin for Bi-De Qin

ACKNOWLEDGEMENTS

I would like to express my deep appreciation to Dr. H. K. Lauw, my major professor, for his teaching, advice, patience and encouragement. I am grateful to Prof. A. Wallace, Prof. J. Davis and Prof. R. Wilson for serving on my graduate committee and for reviewing this thesis. Also, a special thanks to Mr. & Mrs. Larry Lev for their help in reading the manuscript of this thesis.

I would like to take this opportunity to express my hearty thanks to my uncle, Prof. D. G. Chin. The support, understanding and encouragement from him are gratefully appreciated.

I express my sincere appreciation to my wife E Ding and my son Wei for their loves and sacrifices. Finally, to my parents:

Such a tiny blade of grass
Can you ever repay the sunshine of spring ?

SYMBOL LIST

subscripts 1,2 = separate machine sections

f_1, f_2 = frequency of stator quantities, Hz

f_r = frequency of rotor currents, Hz

f_m = rotor speed, Hz

w = angular frequency, rad/s

V_1 ,V_2 = per phase stator supply voltage, V

I_1 ,I_2 = per phase stator currents, A

I_r = per phase rotor current, A

R_1 ,R_2 = per phase stator winding resistance,ohm

R_{r1} ,R_{r2} = per phase rotor winding resistance,ohm

P_{ag} = delivered power from stator to rotor across airgap, W

P_{em} = total input mechanical power, W

P_{em1},P_{em2} = mechanical power into each stator, W

P_{e1} = electrical power out from stator 1, W

P_{e2} = electrical power into stator 2, W

N_1,N_2 = pole pair numbers of each machine section

s = slip

X_1 ,X_2 = per phase stator winding leakage reactance, ohm

X_{r1} ,X_{r2} = per phase rotor winding leakage reactance, ohm

X_{m10} ,X_{m20} = per phase magnetizing reactance, ohm

TABLE OF CONTENTS

LIST OF FIGURES

OPERATING CHARACTERISTICS OF THE BRUSHLESS DOUBLY FED MACHINE

INTRODUCTION

The cascade connection of induction motors was one of the earliest methods used to obtain multi-speed operation of induction motors. The doubly fed wound-rotor motor can operate as a synchronous machine at a specified speed. Rapid developments in power electronics have led to the use of the brushless doubly fed machines (BDFM), or single-frame self-cascade machine, with a power electronic converter as a variable speed generator (Ref.[1]).

In construction the rotor of the brushless doubly fed machine closely resembles a conventional induction motor. The BDFM may be regarded as being electrically equivalent to two separate cascade connected wound-rotor induction machines which are coupled mechanically to the same shaft and load. With constant frequency power applied to the primary winding and variable frequency power (power electronic converter) applied to the secondary winding, a smooth speed variation can be achieved. The BDFM thus operates as an ajustable speed synchronous machine.

When the BDFM is used as a variable speed generator, it is possible to maintain maximum efficiency of the energy-conversion process under varying resource conditions by electronically controlling the shaft speed. How can its steady-state performance best be analyzed ? How can its steady-state stability limits be determined? What are the excitation requirements ? The answers of these questions are very important to assure proper performance of the entire system and the power electronic converter. In the following sections of this thesis a theoretical method for analyzing the performance of a BDFM is discussed, an analysis of its steady-state performance is made, and results of measurements on a practical BDFM in order to verify the theory are presented.

1. RELATED THEORY AND BACKGROUND

1.1 DOUBLY-FED MACHINE

The concept of the doubly fed machine has been recognized for some time. The term " wound rotor machine " is probably more familiar than the term " doubly fed machine". A polyphase wound rotor induction motor with balanced windings on both stator and rotor can operate as a synchronous machine at a specified speed if both stator and rotor are connected to a symmetrical polyphase supply. It can retain this speed over a range of load torque while providing adequate synchronizing torques.

Consider a 2-pole machine with stator and rotor fed respectively by supplies of angular frequency w_1 and w_2. Both stator and rotor produce a travelling wave of m.m.f. around the gap in a direction corresponding to the chosen phase sequence. The interaction torque pulsates at all rotor speeds w_m, except that for which $w_m + w_2 = w_1$. Only when the stator and rotor m.m.f. patterns are synchronized can a sustained unidirectional torque be established. A condition was given by $w_m = w_1 + w_2$, the sign depending on the relative stator and rotor phase sequences. If these are opposite, and if both stator and rotor are

fed at the same supply frequency, the synchronous speed is $w_m=2w_1$; thus a 2-pole 50 HZ motor runs stably at 6000 r/min. The excitation of the air-gap flux is shared by the stator and rotor m.m.f.s just as it is with a conventional synchronous machine in which $w_2=0$ (i.e., a d.c. supply) and $w_m = w_1$. The maximum torque of an a.c. doubly-fed motor is always greater than that of a comparable singly-fed induction machine, and with its high speed represents a very compact power converter.

Thus, a motor with its stator and rotor fed at different frequencies can operate at synchronous speeds corresponding to the sum or difference of the supply frequencies. At the cost of giving up the simplicity of a squirrel-cage induction machine, a wide speed range can be obtained by providing the rotor with slip rings to which a voltage of variable frequency is applied. The cascade topology of the wound-rotor induction motor dispenses with the need to use slip rings for connecting the converter with the rotor windings, and yet the same benefits of a wound-rotor induction machine are expected.

1.2 CASCADE CONNECTED MACHINE

Control by means of the cascade topology of induction motors is fundamentally one of the earlier methods of slip control through a secondary " foreign " voltage. It has long been known as a means by which low speeds of operation can be obtained. It was developed independently in 1893 by Steinmetz in the U.S.A. and Görges in Germany. The cascade topology of induction motors improves the overall efficiency as compared to the variable rotor resistance method of speed control in which the slip power is dissipated in resistance losses. In the cascade connection the slip power is either returned to the supply network or is used to drive an auxiliary motor which is mechanically coupled to the induction motor shaft.

In the cascade scheme, two wound-rotor induction motors are coupled mechanically to the same shaft and load. The secondary winding of the supply machine is connected to the primary winding of the second machine and electrically in reversed phase sequence. The balanced currents circulating in the two sets of windings will set up rotating fields in each machine having opposite directions of rotation with respect to the shaft. If the first motor has $2N_1$ poles and the second motor $2N_2$ poles, the cascade

connection machine acts like a $2(N_1+N_2)$-pole machine. Therefore, the operation of the cascade connection motor can be regarded as speed control by e.m.f. injection in the rotor circuit of a wound-rotor induction machine. With constant frequency power applied to the primary winding of the supplied machine, and variable frequency power (the power electronic converter) applied to the secondary winding of the second machine, a smooth speed variation can be achieved.

1.3 BRUSHLESS DOUBLY FED MACHINE

There were several attempts to develop a "single-unit " cascade machine, i.e. a self-cascaded single-frame machine, to achieve improved performence and reduced cost. The " Hunt motor " invented by J.L.Hunt, and later developed by Creedy, was the most notable of these and the first to achieve some commercial success. Various winding configurations are possible for the cascade machine built on one set of laminations. Two separate winding arrangements in which both the rotor and stator have two sets of winding of different pole numbers result in low utilization of the slot space. Single windings have the advantage of increasing the conductor area of the stator winding

resulting in reduced copper losses and higher efficiency, etc.(Ref.[2]) The self-cascade single-frame machine will here be denoted by Brushless Doubly Fed Machine (BDFM) because both 3-phase systems on the stator will be connected to external frequency sources.

Because of the single-unit construction the BDFM closely resembles a conventional induction machine. It may still be regarded as a special doubly-fed machine. The terminals of one of the stator 3-phase systems are connected to the constant frequency supply, while the other stator 3-phase system is connected to a power electronic converter which also provides a constant frequency supply. The BDFM may be run asynchronously with resistance control if required, or synchronously without any external connections to the "rotor" winding. It has the advantage of a compact and robust form of rotor construction, without slip rings or rotating diodes, and requires minimum maintenance. By the use of modern power electronic converters, the machine is ideally suited for operation as an adjustable speed brushless alternator to convert electric energy from erratic energy resources such as wind, solar, and hydro.

2. STEADY-STATE ANALYSIS OF THE BDFM

2.1 OPERATING MODES OF THE BDFM

2.1.1 SINGLY-FED MODE

The brushless doubly fed machine may be run in the singly-fed mode as a variable speed machine with resistance for speed control if required. Instead of using external resistances to dissipate the slip power, a rectifier-inverter (DC-link converter) can be used to return the slip-frequency power to the line. For sub-synchronous speed control the primary stator winding is connected to the supply line and the secondary stator winding to the solid state rectifier-inverter, as shown in Fig.2.1. The slip power from the rotor circuit is transferred by induction to one set of stator windings. A three phase bridge rectifier, which operates at slip frequency, feeds rectified slip power through the smoothing inductor to the thyristor inverter. The inverter returns the slip power to the a.c. supply.

For the DC-link converter the average counter e.m.f. of the inverter may be regarded as an injected e.m.f. opposing the rectified "rotor" voltage. If commutation overlap is negligible, the direct voltage output (V_{do}) of the uncontrolled three-phase bridge rectifier is obtained as

$$V_{do}=1.35V_r\ s \quad \ldots\ldots\ldots\ldots\ldots\ldots\ldots\ldots(1)$$

where V_r is the line-to-line "rotor" voltage at standstill and s is the fractional slip.

For a three phase bridge inverter the average counter e.m.f. is given by

$$V_d=1.35\ V_l \cos Á \quad \ldots\ldots\ldots\ldots\ldots\ldots\ldots\ldots(2)$$

where Á is the firing delay ($Á \geq 90^{\circ}$), and V_l is the a.c. line voltage.

On a no-load setting the motor torque is negligible and the rectifier "rotor" current is almost zero. Consequently, the two direct voltages of equations (1) and (2) must balance;

thus

$$1.35\ V_r\ s + 1.35\ V_l \cos Á = 0$$

or

$$s = -(V_l/V_r) \cos Á = - a \cos Á = a \left|\cos Á\right| \ldots(3)$$

where a is the effective "stator-to-rotor" turns ratio of the BDFM.

No load speed control is, therefore, obtained by a simple variation of the inverter firing angle.

In order to develop load torque, a "rotor" current I_2 is required, and the rectified "rotor" voltage must force current flow against the inverter back e.m.f.. As the motor is loaded the speed falls slightly and the resulting increase in rectified voltage produces the necessary increase in "rotor" current.

In order to bring out the essential points of performance in as clear a manner as possible, the "rotor" losses are neglected. Thus the fundamental "rotor" slip power, sP_{ag}, is approximately equal to the d.c. link power:

$$s\,P_{ag} = V_d\,I_d\ ,$$

where I_d is the rectified "rotor" current.

Since $P_{ag} = T\,w_m$,

where T is the electromagnetic torque developed by the BDFM, and w_m is the synchronous angular velocity,

hence $T = V_d I_d / s w_m$.

If the speed droop on load is neglected, equation (3) for the no-load slip can be substituted in this result. Substituting also for V_d from equation (2) gives the toque expression

$$T = 1.35\,V_1\,I_d\,/a\,w_m\ .$$

Thus, the steady-state torque is proportional to the rectified "rotor" current, I_d, which is proportional to the difference between the rectified "rotor" voltage and the average counter e.m.f. of the inverter.

The principal disadvantage of the sub-synchronous cascade drive is its low fundamental power factor or displacement factor. This low power factor is partly due to the commutating reactive power which is drawn through the induction motor from "stator" to "rotor" by the three phase rectifier. However, the reactive power consumption of the phase controlled inverter is also partially responsible for the low power factor of the cascade drive.

Several circuit modifications have been devised in order to improve the power factor of the cascade drive.(Ref.[3],[4],[5])

In a sub-synchronous cascade drive which is controlled from standstill to full speed, the static converter must have the same KVA rating as the BDFM. When the sub-synchronous speed range is limited, however, the converter rating is reduced proportionally and the system power factor is improved. (Ref.[4])

2.1.2 DOUBLY-FED MODE

When balanced polyphase supplies are connected to the primary and secondary windings of the BDFM it may operate synchronously at speeds proportional to the sum or difference of the supply frequencies. Loss of synchronism does not require shut down of the system. Loss of synchronizm only results in the asynchronous (induction) mode of operation.In this case the rotor currents carry two component frequencies. Moreover, the machine efficiency will be low since the torques produced by the two 3-phase system will be counteractive. Thus, the synchronous mode is preferred. The speed at which the BDFM operates is determined by the relative phase sequences of the primary and secondary winding supply frequencies. Such operating mode is called doubly-fed (synchronous) mode. With constant frequency power applied to the primary stator winding (e.g.,6-pole) and variable frequency power (static power electronic converter) applied to the secondary stator winding (e.g.,2-pole) a smooth speed variation can be achieved. The BDFM operates as an adjustable speed synchronous machine as shown in Fig.2.2.

Using the BDFM as an adjustable speed synchronous machine is a major application of this kind of machine. Rapid developments in modern power electronics may lead to the potential of utilizing the BDFM with a power electronic converter as a variable speed generation (VSG) system which can be expected to be more effective than the conventional fixed-speed system for generation of electric energy from variable energy sources such as hydro, wind or solar. The most important benefit of the variable-speed generation system is its potential for electronically controlling the shaft-speed in order to maintain maximum efficiency of the energy conversion process, irrespective of varying resource conditions.

As several authors indicated, the doubly-fed machine is inherently unstable in certain speed regions depending on the parameters of the machine (Ref.[8],[9]). The machine in such a case produces an electromagnetic torque component which in effect causes the machine to be subjected to a negative damping torque. It is possible to adjust certain machine parameters such that this negative damping torque would be prohibited from becoming dominant. Another way to overcome the inherent instability of the doubly-fed machine is including a stabilizer in the VSG system controller in order to compensate for negative torques.

It was also recently demonstrated [1] that the stability problem is contained if a power electronic converter with a current-source character is used. Such a converter type is the series-resonant converter. This kind of converter was used in our laboratory-scale (15 KW) variable-speed generation system in which the BDFM is used as an adjustable-speed synchronous machine.

The series-resonant converter interfaced to our laboratory VSG system exhibits all the crucial functional capabilities; which include: four quadrant and bidirectional power flow, controllable output amplitude and frequency with a range of -80 HZ to +80 HZ, no demand for reactive power from the input power supply irrespective of the loading condition, and no use of low-order harmonic filters. The results of measurements indicated that the harmonics generated by a VSG system using a series-resonant converter are significiantly lower than those generated by a VSG using a DC-link converter which can be expected to generate considerably less harmonics than the cycloconverter. The cycloconverters are nevertheless favored for use in the VSG system since DC-link converters are not capable of providing a smooth transition at zero frequency. It can be demonstrated that the series-resonant converter does provide this transition at zero frequency.

Another advantage of the series-resonant converter is that it is capable of operating in either the programmable voltage-source mode or the programmable current-source mode in order to provide the excitation power to the BDFM. These source modes are programmable in the amplitude and the frequency. The performance of the VSG system was compared for the two modes. As compared to the current-source mode, the total harmonic distortion on both the stator current and the rotor current will be significiantly increased if the converter is operated in the voltage-source mode. As mentioned earlier, inclusion of a stabilizer in the VSG system controller was proposed in order to compensate negative damping torques. However, an eigenvalue analysis did confirm that unstable modes could be eliminated with a current-source excitation of the " rotor windings ". Thus the use of the current-source mode dispenses with the need to include a stabilizer. The above factors lead to the conclusion that the current-source mode should be preferred to the voltage-source mode.

The BDFM, from an operational point of view, behaves more like a synchronous machine. Its operating characteristics under the synchronous mode are very important in determining the performance of the VSG

system and the power electronic converter. In the following sections the steady-state performance analysis of the BDFM under the synchronous mode will be given. Further, a convenient tool for analyzing the operating characteristics will be presented. This analytical tool can be developed into efficient supervisory control logic to assure proper operation under varying resource conditions.

2.2 STEADY-STATE PERFORMANCE OF THE BDFM UNDER SYNCHRONOUS MODE

2.2.1 THE GENERAL EQUIVALENT CIRCUIT OF THE BDFM

The basis of the present analysis is a circle diagram method. Only the steady-state performance is considered. The analysis is made on a per-phase basis, assuming a balanced polyphase machine having a uniform air gap and balanced polyphase supply.

In construction, the BDFM closely resembles a conventional induction machine. However the steady-state performence of the BDFM may be analyzed by considering two separate cascade connected wound-rotor actions in the usual way. A system with two wound-rotor induction machines with their rotors coupled mechanically and electrically in reversed sequence will be considered. This means that balanced currents

circulating in the two sets of stator windings will set up rotating fields in each machine, having opposite directions of rotation with respect to each other.

Electrically, the BDFM is equivalent to two separate cascade connected wound rotor induction machines. The equivalent circuit representing the BDFM with different frequency supplies is given in Fig.2.3 which is a cascade of two well-known equivalent diagrams of induction machine. The rotor voltage of the first machine is not shorted, but is equal to the rotor voltage of the second machine. The stator voltage of the second machine is equal to the external voltage supplied by the power electronic converter divided by the slip s with respect to $2N_1$-pole field.

The relation between f_1, f_2 and f_m under synchronous mode is shown in Fig.2.4. The relationship between the slip, supplied frequencies and the pole numbers can be obtained from follows:

$$f_1 = f_r + N_1 f_m \ ,$$

$$f_2 = f_r - N_2 f_m \ ,$$

$$f_m = \frac{f_1 - f_2}{N_1 + N_2} = \frac{(1-s)\ f_1}{N_1 + N_2} \ ,$$

with:

$$s = (f_1-(N_1+N_2)f_m)/f_1 = f_2/f_1 \quad ,$$

$$s = s_1\, s_2 \quad ,$$

$$s_1 = f_r/f_1 \quad , \quad s_2 = f_2/f_r \quad .$$

In order to bring out the essential points of performance in as clear and concise a manner as possible, the core losses, R_{m10} and R_{m20}, are neglected. Under this assumption the equivalent circuit of the BDFM becomes as shown in Fig.2.5.

It is to be noted that in the induction mode the rotor windings will carry two frequencies. In this case:

$$s = (f_2/f_1)*(f_{r1}/f_{r2}) \quad ,$$

with:

$$s_1 = f_{r1}/f_1 \quad ; \quad s_2 = f_2/f_{r2} \quad .$$

2.2.2 POWER BALANCE WITHIN THE BDFM

Based on the generator convention, the power flow in the BDFM is shown in Fig.2.6. Of the air-gap power P_{ag}, i.e. the amount of power passing across the airgap from the stator to rotor, only a fraction (1-s) P_{ag} originated from the mechanical input power. From Fig.2.5 and Fig.2.6 the power relationship in the BDFM can be obtained as follows.

The total power balance of the BDFM is

$$P_{em} + P_{e2} = (I_2^2 R_2 + I_r^2 R_{r2}) + (I_1^2 R_1 + I_r^2 R_{r1}) + P_{e1} ,$$

where $I_2^2 R_2$ and $I_r^2 R_{r2}$ are respectively stator and rotor copper losses of machine 2 , and $I_1^2 R_1$ and $I_r^2 R_{r1}$ are respectively stator and rotor copper losses of machine 1 .

The power balance for machine 2 is

$$(P_{e2} - I_2^2 R_2) + P_{em2} = P_{ag2} ,$$

with $P_{em2} = (1-s_2) P_{ag2}$,

$P_{ag2} = I_r^2 R_{r2} + P_{er}$,

where P_{er} is the slip power from the rotor of machine 2 transfered to the rotor of machine 1.

The power balance for machine 1 is

$$P_{em1} + (P_{er} - I_r^2 R_{r1}) = P_{ag1} \ ,$$

with $P_{ag1} = I_1^2 R_1 + P_{e1}$,

$P_{em1} = (1-s_1) P_{ag1}$.

It is clear that

$$P_{em} = P_{em1} + P_{em2} = (1-s_1) P_{ag1} + (1-s_2) P_{ag2} \ .$$

The power balance within the BDFM can be visualized as shown in Fig.2.7.

In order to obtain the essential power relationship of the BDFM the losses are neglected, i.e.

$$I_1^2 R_1 = I_2^2 R_2 = I_r^2 (R_{r1}+R_{r2}) = 0 \ .$$

Hence $P_{ag2} = s_1 P_{ag1}$,

$P_{ag1} = P_{e1}$,

$P_{e2} = s_2 P_{ag2}$.

Therefore

$$P_{e2} = s P_{e1} \ .$$

The following important equation can be obtained from the above equations:

$$Pem = Pe1 - Pe2 \quad .$$

This equation is useful in determining the excitation requirements for a given characteristic of Pm= f(wm).

If the losses are negligible, the essential distribution of mechanical power between the two cascade machines can also be inferred from the following relation:

$$\frac{Pem2}{Pem1} = \frac{Tem2}{Tem1} = \frac{(1-s2)\ Pag2}{(1-s1)\ Pag2} \approx \frac{N2}{N1} \quad .$$

The single-phase equivalent circuit Fig.2.5 obviously captures the essential steady-state performance features of the BDFM, but it fails to transparently provide the correlation of the variables which are crucial to the characteristics of the operating modes. A powerful tool for this purpose is the circle diagram method, which can be derived from the same voltage and current relations reflected by the equivalent circuit. It will be explained that the diagram provides the opportunity to characterize or

correlate all important variables for any operation mode.

2.2.3 CIRCLE DIAGRAM ANALYSIS OF THE BDFM

The use of the circle diagram method to analyze the steady-state performance of a doubly-fed machine was described in Ref.[1]. This method can be also applied to determine the operating characteristics of the BDFM, evaluate the stability limits and excitation requirements, and establish the correlation of the variables in a convenient manner. In other words, a desired or undesired change of a target operating mode can be immediately evaluated by tracing the trajectory of the change in the circle diagram.

The circle diagram can be derived from the voltage and current relations which are reflected by the equivalent circuit. Note that the equivalent circuit of the BDFM is different from that of the doubly-fed machine. This difference will cause the circle diagram parameters of the BDFM to be dependent on the speed of machine. In order to expediently apply the circle diagram method to the BDFM , a network simplification of the equivalent circuit of the BDFM should be made.

Since the BDFM will be controlled by I_2 and f_2 , it is necessary to have these variables reflected in the circle diagram.

By the application of Thevenin's theorem and network simplification the equivalent circuit of the BDFM shown in Fig.2.5 can be converted to an alternative form which is shown in Fig.2.8. The alternative form is similar to that of a conventional doubly-fed machine, but the parameters of the BDFM will be dependent on the speed, i.e. the slip s.

The relationships between the parameters shown in Fig. 2.5 and Fig. 2.8 are:

$$\bar{V}_1{}^{th} = \frac{jX_{m10}}{R_1+j(X_{m10}+X_1)}\,\bar{V}_1 \quad ,$$

$$\bar{I}_1{}^{th} = \bar{I}_r \quad ,$$

$$\bar{S} = \bar{V}_1\bar{I}_1{}^* = \bar{V}_1{}^{th}\bar{I}_1{}^{th*} \quad ,$$

$$Z_1{}^{th} = R_1{}^{th} + jX_1{}^{th} \quad ,$$

where

$$R_1{}^{th} = \frac{R_1\,X_{m10}{}^2}{R_1{}^2+(X_{m10}+X_1)^2} \quad ,$$

$$X_1{}^{th} = \frac{X_{m10}(R_1{}^2+X_1{}^2+X_1\,X_{m10})}{R_1{}^2+(X_{m10}+X_1)^2} \quad .$$

In fact, $R_1 << (X_{m10}+X_1)$, so the assumption

$$\frac{jX_{m10}}{R_1+j(X_{m10}+X_1)} = \frac{X_{m10}}{X_{m10}+X_1}$$

is reasonable.

Hence, $$\bar{V}_{1th} = C_{th}\bar{V}_1 ,$$

$$\bar{I}_{1th} = \bar{I}_r = \frac{\bar{I}_1}{C_{th}} ,$$

where $$C_{th} = \frac{X_{m10}}{X_{m10}+X_1} .$$

From this assumption, the alternative quivalent circuit of Fig.2.8 is simplified to the circuit as shown in Fig.2.9.

In Fig.2.9, $$\bar{V}_{e1} = C_{th}\bar{V}_1 ,$$

$$\bar{I}_{e1} = \frac{\bar{I}_1}{C_{th}} = \bar{I}_r ,$$

$$R_{e1} = R_1{}^{th}{}_+ \frac{R_{r1}+R_{r2}}{s_1} ,$$

$$X_{e1} = X_1{}^{th}{}_+ X_{r1}+ X_{r2} .$$

Fig.2.9 is similar to the equivalent circuit of the conventional doubly-fed machine, but the parameter R_{e1} is dependent on the slip s_1. Therefore, the BDFM

can be considered as a "doubly-fed" machine. Its "stator" terminal is 1-1′, and its "rotor" terminal is 2-2′.

From the equivalent circuit of the BDFM shown in Fig.2.9 the "stator" and "rotor" voltage eqations can be obtained as follows.

$$\bar{V}_{e1} = - Z_{e1}\bar{I}_{e1} + \bar{E}_r \quad \cdots\cdots\cdots\cdots\cdots \quad (4)$$

$$\frac{\bar{V}_2}{s} = \left(\frac{R_2}{s} + j(X_2+X_{m20})\right) \bar{I}_2 - j\, X_{m20}\, \bar{I}_{e1} \quad \cdots \quad (5)$$

Assume that the phase angle of the "stator" terminal voltage is taken as zero, i.e.

$$\bar{V}_1 = V_1\, e^{j0} ,$$

hence $$Z_{e1} = R_{e1} + j(X_{e1}+X_{m20}) = j\, z_{e1} e^{-j\alpha_{e1}} ,$$

$$z_{e1} = Z_{e1} = \{ R_{e1}^2 + (X_{e1}+X_{m20})^2 \}^{1/2},$$

$$\alpha_{e1} = \tan^{-1}\left(\frac{R_{e1}}{X_{e1}+X_{m20}}\right) ,$$

$$\bar{E}_r = jX_{m20}\bar{I}_2 = E_r\, e^{j\delta} ,$$

$$E_r = X_{m20}\, I_2 ,$$

$$\bar{I}_2 = I_2\, e^{j\theta} ,$$

$$\delta = \frac{\pi}{2} + \theta \quad .$$

From equation (4) the current $\bar{I}_{e1}$ can be obtained

$$\bar{I}_{e1} = \frac{X_{m20}}{z_{e1}} I_2 e^{j(\delta+\alpha_{e1}-\frac{\pi}{2})} + \frac{V_{e1}}{z_{e1}} e^{j(\frac{\pi}{2}+\alpha_{e1})} \quad \ldots\ldots\ldots\ldots\ldots\ldots\ldots (6)$$

In accordance with equation (6), the "stator" current phasor diagram can be drawn and is shown in Fig.2.10. The coordinates of the point N are

$$N = \left(-\frac{V_{e1}}{z_{e1}} \sin(\alpha_{e1}), \frac{V_{e1}}{z_{e1}} \cos(\alpha_{e1}) \right) .$$

The trajectory for operating modes with a constant value of the rms "rotor" current I_2 is a circle with point N as the center and a radius equal to the product of the rms value and a coefficient Γ_2 . Unlike the conventional doubly fed machine, this coefficient Γ_2 is not constant; it depends on the speed of the BDFM. For a specified speed, Γ_2 is a constant. For any given machine, Γ_2 can be calculated from the relationship:

$$\Gamma_2 = \frac{X_{m20}}{z_{e1}} \quad , \quad \text{where} \quad z_{e1} = \{ R_{e1}^2 + (X_{e1}+X_{m20})^2 \}^{1/2}.$$

Therefore, for any given BDFM the curve of $\tilde{a}_2$ versus slip s can be drawn as in Fig.4.4.

If the "stator" or "rotor" voltage equations are respectively multiplied by the "stator" or "rotor" current phasors, then the resulting equations represent the power balance which can be graphically reflected on the phasor diagram as well.

Multiplying equations (4) and (5) by the "stator" and "rotor" conjugate currents $\bar{I}_{e1}^*$ and $\bar{I}_2^*$ respectively, we can derive following relationships:

$$3\,\bar{V}_{e1}\bar{I}_{e1}^* = -3[R_{e1}+j(X_{e1}+X_{m20})]\,I_{e1}^2+3jX_{m20}\bar{I}_2\bar{I}_{e1}^* \quad \ldots\ldots\ldots\ldots\ldots\ldots\ldots\ldots(7)$$

$$\frac{3\,\bar{V}_2\bar{I}_2^*}{s} = 3[\frac{R_2}{s}+j(X_2+X_{m20})]\,I_2^2- 3jX_{m20}\bar{I}_{e1}\bar{I}_2^* \quad \ldots\ldots\ldots\ldots\ldots\ldots\ldots\ldots(8)$$

By taking the real part of the above equations the active power balance can be obtained.

$$3\,\mathrm{Re}\{\,\bar{V}_{e1}\bar{I}_{e1}^*\} = -3R_{e1}I_{e1}^2+ 3\mathrm{Re}\{\,jX_{m20}\bar{I}_2\bar{I}_{e1}^*\,\} \quad \ldots\ldots(9)$$

$$3\,\mathrm{Re}\{\frac{\bar{V}_2\bar{I}_2^*}{s}\} = 3\,\frac{R_2I_2^2}{s} - 3\mathrm{Re}\{\,jX_{m20}\bar{I}_{e1}\bar{I}_2^*\,\} \ldots\ldots(10)$$

i.e.

$$P_{e1} = -P_{R1}+ P_{ag} \quad \ldots\ldots\ldots\ldots\ldots\ldots(11)$$

$$P_{e2} = P_{R2} + sP_{ag} \quad \ldots\ldots\ldots\ldots\ldots\ldots(12)$$

where

$P_{ag} = 3\mathrm{Re}\{\,jX_{m20}\bar{I}_2\bar{I}_{e1}^*\,\} = -3\mathrm{Re}\{\,jX_{m20}\bar{I}_{e1}\bar{I}_2^*\,\}$,

$P_{e1} = 3\mathrm{Re}\{\,\bar{V}_{e1}\bar{I}_{e1}^*\,\} = 3V_{e1}I_{e1}\cos(\Phi_1)$,

$$P_{e2} = 3\mathrm{Re}\{ \bar{V}_2 \bar{I}_2^{*} \} = 3V_2 I_2 \cos(\Phi_2) \ ,$$

$$P_{R1} = 3R_{e1} I_{e1}^{2} \ ,$$

$$P_{R2} = 3R_2 I_2^{2} \ ,$$

P_{ag} is the equivalent airgap power of the BDFM.

The total power balance is given by:

$$P_{em} + P_{e2} = P_{R1} + P_{R2} + P_{e1} \quad \ldots\ldots\ldots\ldots (13)$$

Substituting (11) and (12) into (13), we get

$$P_{em} = (1-s)\ P_{ag} \quad \ldots\ldots\ldots\ldots\ldots\ldots (14)$$

It was mentioned earlier that only a fraction of the equivalent air-gap power P_{ag} flows across the airgap from "stator" to "rotor", i.e. the fraction $(1-s)P_{ag}$ originates from mechanical input power. This equation is important for establishing the operating point of the BDFM for given characteristics of the mechanical inputs, i.e. $P_{em}=f(w_m)$.

By taking the imaginary part of equations (7) and (8) the reactive power balance can be also obtained from the following equations:

$$Q_{e1} = -Q_{xe1} + Q_{ag} \quad \ldots\ldots\ldots\ldots\ldots\ldots (15)$$

$$Q_{e2} = sQ_{x2} - sQ_{ag} \quad \ldots\ldots\ldots\ldots\ldots\ldots (16)$$

$$Q_{em} = (1+s)\ Q_{ag} \quad \ldots\ldots\ldots\ldots\ldots\ldots (17)$$

where

$$Q_{ag} = 3\mathrm{Im}\{ jX_{m20}\bar{I}_2\bar{I}_{e1}^{*}\} ,$$

$$Q_{xe1} = 3(X_{e1}+X_{m20}) I_{e1}^{2} ,$$

$$Q_{x2} = 3(X_2+X_{m20}) I_2^{2} ,$$

$$Q_{e1} = 3V_{e1}I_{e1} \sin(\Phi_1) ,$$

$$Q_{e2} = 3\mathrm{Im}\{ \bar{V}_2\bar{I}_2^{*}\} .$$

To determine the operating point of the BDFM for given mechanical input conditions we consider equation (9) again.

Writing equation (9) as

$$3 V_{e1}I_{e1}\cos(\Phi_1)= -3 R_{e1}I_{e1}^{2}+ P_{ag} \quad \ldots\ldots\ldots\ldots(18)$$

and substituting the relation

$$I_{e1}^{2} = (I_{e1}\sin(\Phi_1))^2 + (I_{e1}\cos(\Phi_1))^2$$

into equation (18), yield the relationship:

$$(I_{e1}\cos(\Phi_1)+\frac{V_{e1}}{2R_{e1}})^2+(I_{e1}\sin(\Phi_1))^2 =(\frac{V_{e1}}{3R_{e1}})^2+\frac{P_{ag}}{3R_{e1}}$$

Therefore, I_{e1} must lie on a circle with center M, located at a distance ($V_{e1}/2R_{e1}$) from the origin o of the phasor $\bar{V}_{e1}$ as shown in Fig.2.11. The radius of the circle is

$$Rad1 = \left\{ \left(\frac{V_{e1}}{2R_{e1}}\right)^2 + \left(\frac{P_{ag}}{3R_{e1}}\right) \right\}^{\frac{1}{2}}.$$

Let $OM = V_{e1}/2R_{e1}$, consider the circle with M as center and radius OM . This circle represents the current I_{e1} locus for $P_{ag} = 0$. Any smaller circle on center M represents the current I_{e1} locus for some constant airgap power $P_{ag} < 0$. This corresponds with the motor mode. Any bigger circle on center M represents the current I_{e1} locus for some constant airgap power $P_{ag} > 0$. This corresponds with the generator mode.

Applying the same procedure to the "rotor" equation (10) gives

$$\left(I_2\cos(\Phi_2) - \frac{V_2}{2R_2}\right)^2 + \left(I_2\sin(\Phi_2)\right)^2 = \left(\frac{V_2}{2R_2}\right)^2 - \frac{sP_{ag}}{3R_2} \qquad \text{.....(19)}$$

This equation means that the current I_2 must lie on a circle with center M located at a distance $(V_2/2R_2)$ from the origin o of the phasor $\bar{V}_2$, as shown in Fig.2.12.

From equation (19) the minimum V_2 can be obtained

$$V_{2min} = 4sR_2 P_{em}/(3(1-s)) \quad \ldots\ldots\ldots\ldots\ldots\ldots (20)$$

2.2.4 CONDITION FOR SYNCHRONOUS MODE

As mentioned earlier, for a constant value of the rms I_2, the trajectory for operating mode is a circle with point N as center and a radius equal to the product $\Gamma_2 I_2$ as shown in Fig.2.10, and for a constant electromagnetic torque (or airgap power, since the airgap power and the electromagnetic torque are related to each other by a constant factor, i.e. $T_{em} = (N_p/w) P_{ag}$, $T_{em} = T_t$ (input torque), where P_{ag} is determined by the input torque) the trajectory for operating mode is a circle with point M as center and radius equal to Rad_1 as shown in Fig.2.11. Therefore, these two kinds of trajectories are particularly crucial in the sense that a stable steady-state condition (i.e. synchronous mode) is only possible if these two trajectories intersect. For given operating conditions the intersections of these two circles can be found by the circle diagram method above. Therefore, the operating point of the BDFM uder given operating conditions can be uniquely determined as shown in Fig.2.13. If there is no intersection of these two circles the operation of the BDFM is unstable.

By using the circle diagram method, the stable regions of the rms "rotor excitation" current I2 for steady-state operation of the BDFM under given operating conditions can easily be determined. These are shown in Fig.2.14.

In Fig.2.14, the maximum and minimum rms values of the "excitating current" I_2 are

$$I_{2max} = \frac{z_{e1}}{X_{m20}} (Rad_2)_{max} \quad \ldots\ldots\ldots\ldots\ldots (21)$$

$$I_{2min} = \frac{z_{e1}}{X_{m20}} (Rad_2)_{min} \quad \ldots\ldots\ldots\ldots\ldots (22)$$

where $(Rad_2)_{max} = Rad_1 + \{ (M+X_n)^2 + Y_n^2 \}^{1/2}$,

$(Rad_2)_{min} = Rad_1 - \{ (M+X_n)^2 + Y_n^2 \}^{1/2}$,

(X_n, Y_n) are the coordinates of the point N.

(0,M) are the coordinates of the point M.

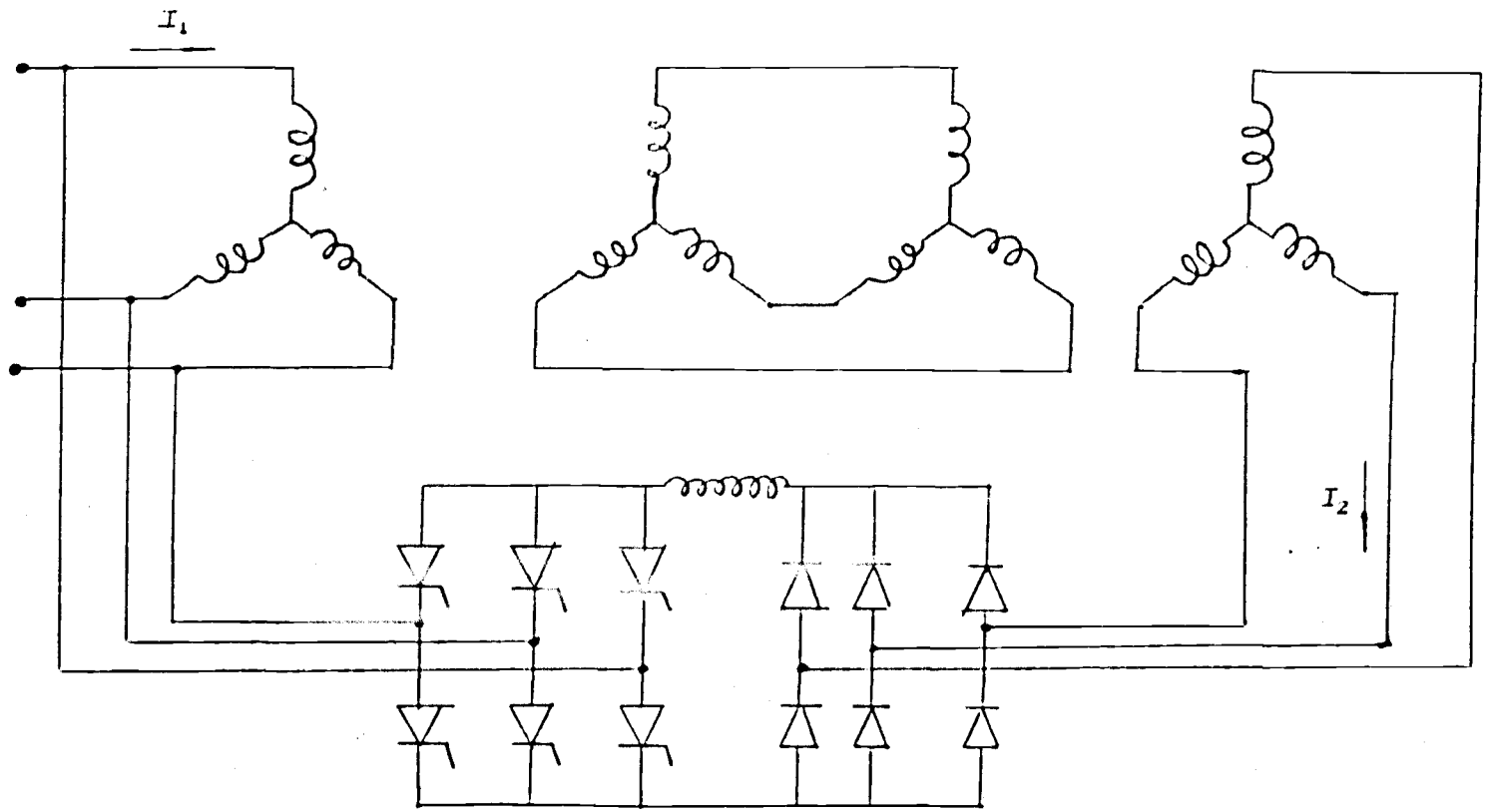

Fig.2.1 The BDFM run asynchronously as a variable speed machine

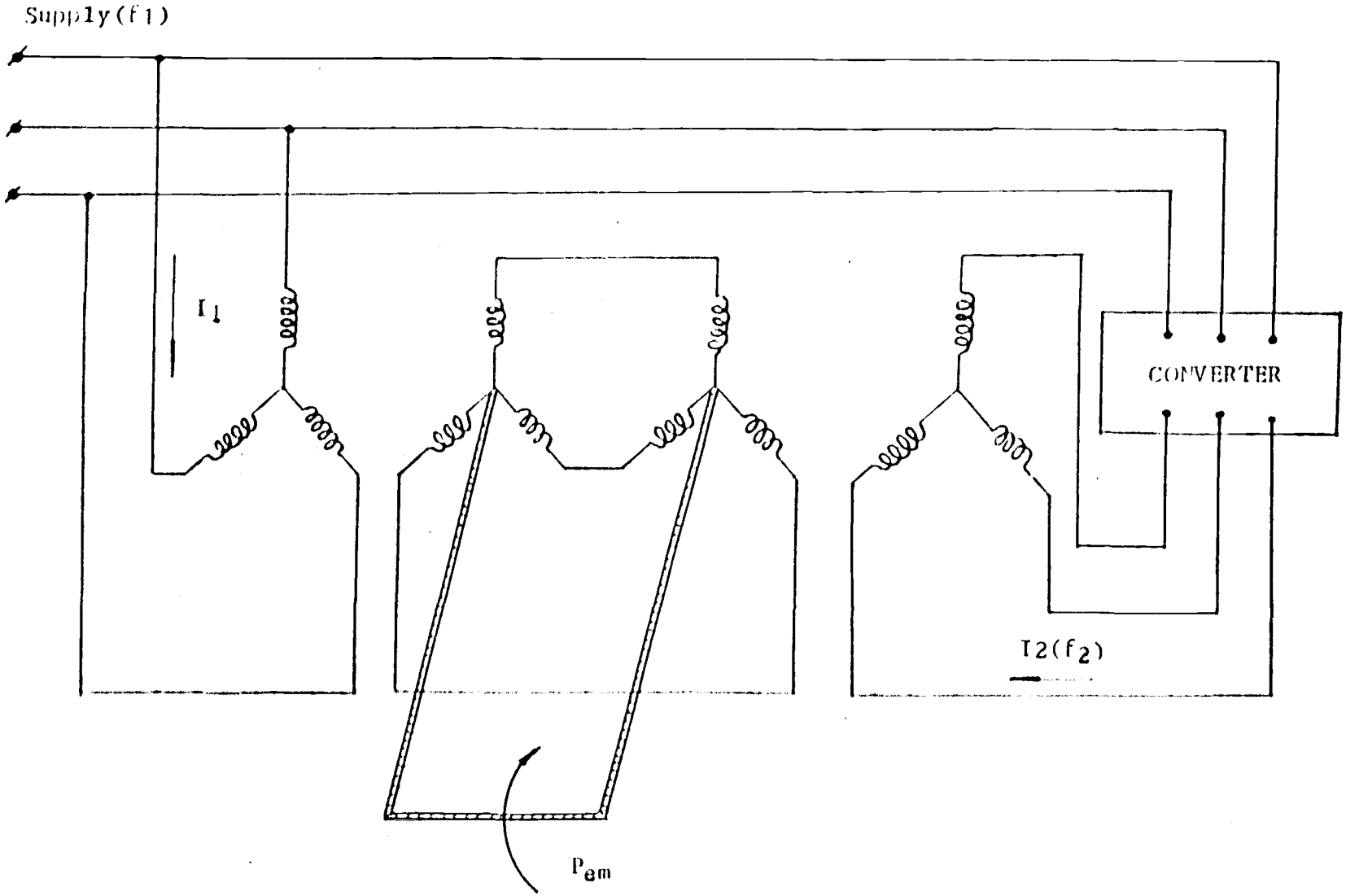

Fig.2.2 The BDFM run synchronously as a variable speed machine

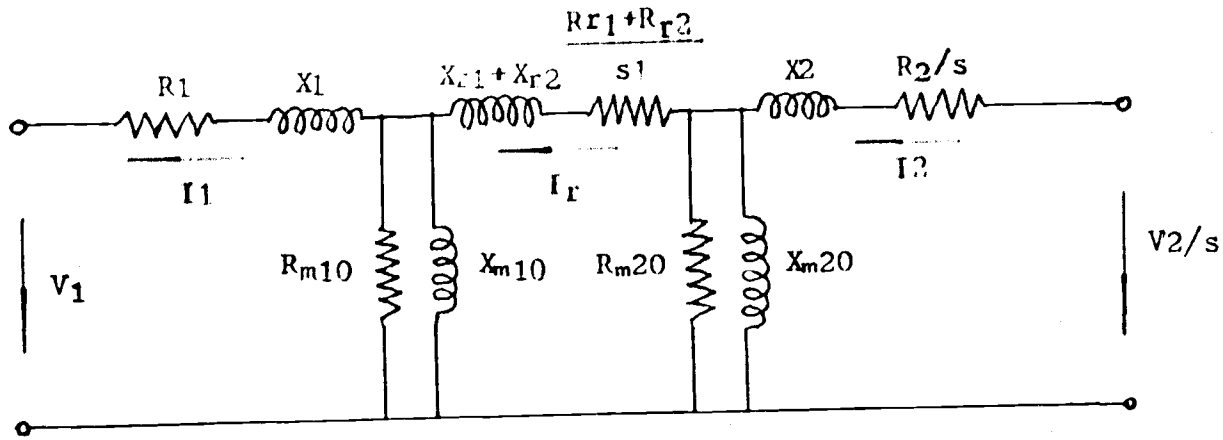

Fig.2.3 Equivalent circuit of the BDFM

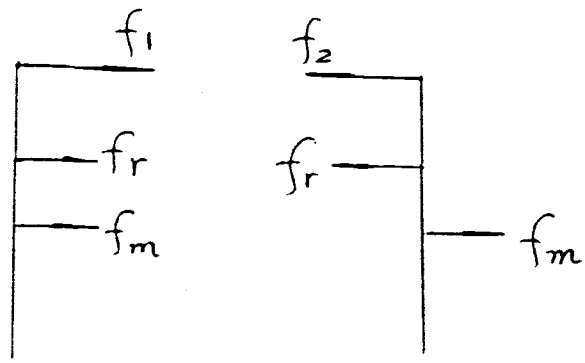

Fig.2.4 Relationship between f_1, f_2 and f_m under synchronous mode

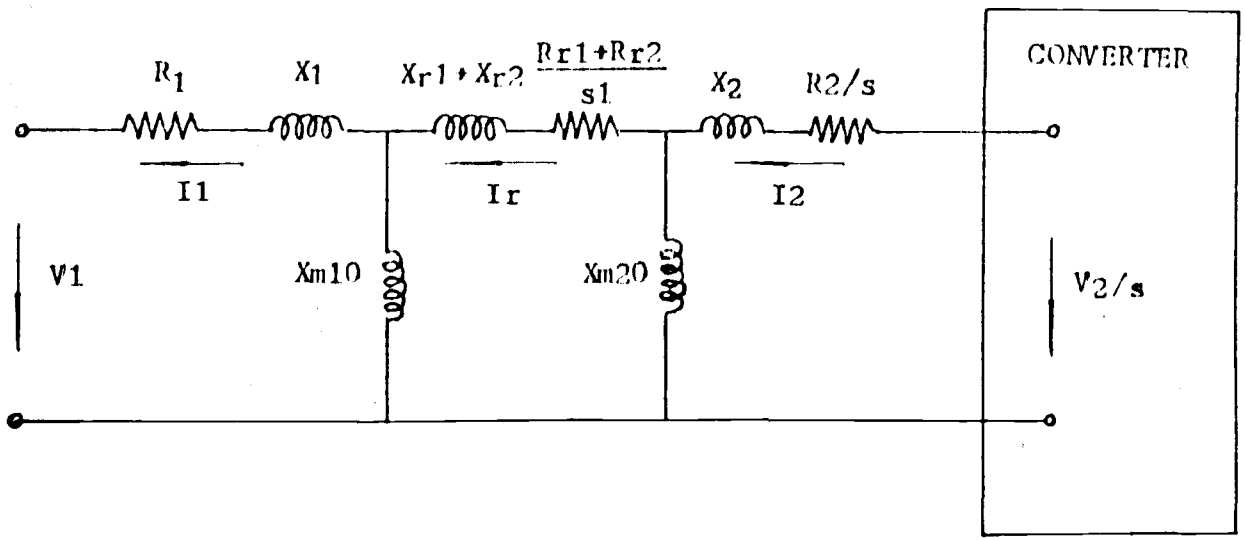

Fig.2.5 Equivalent circuit of the BDFM

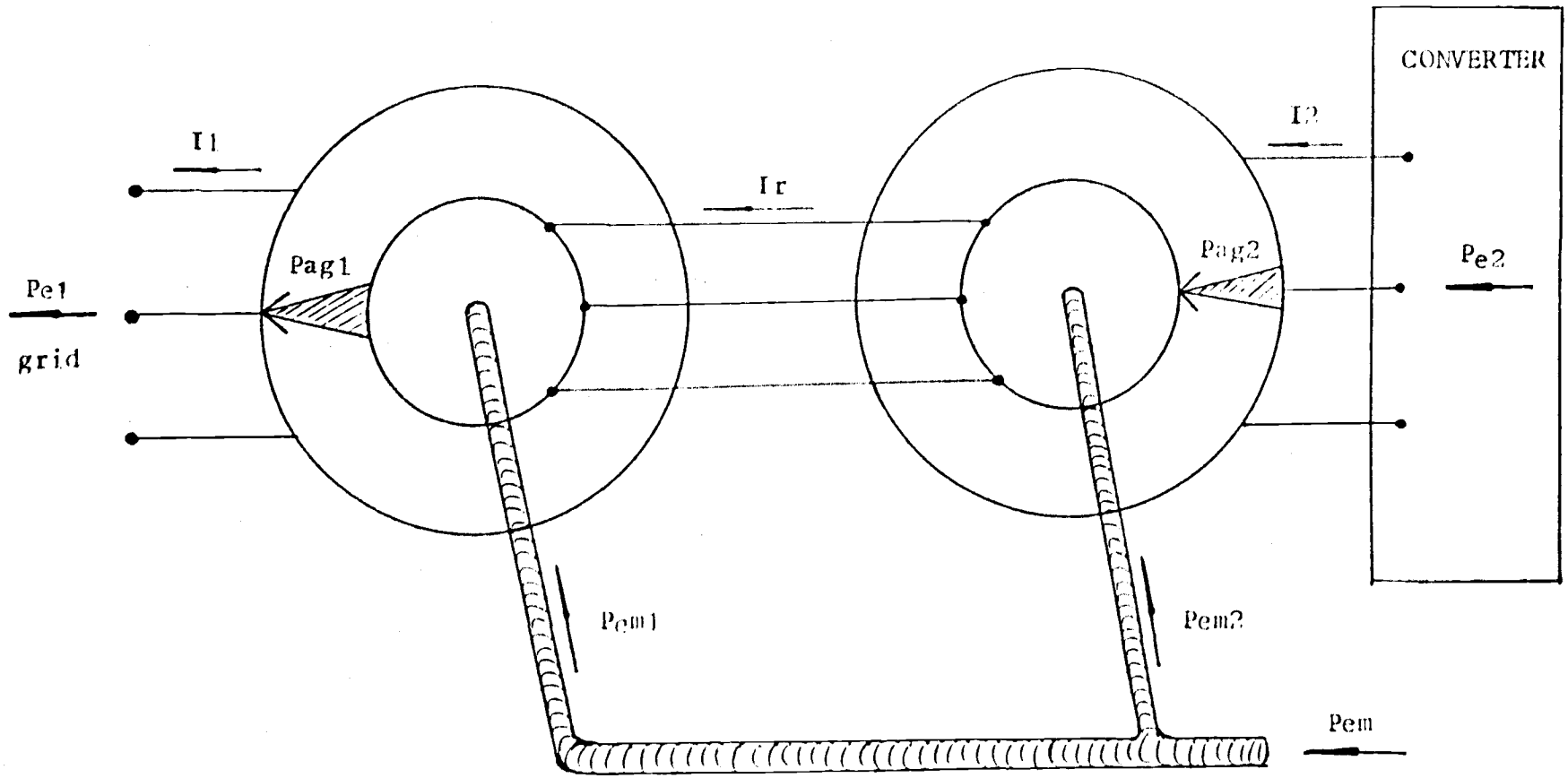

Fig.2.6 Power flow in the BDFM

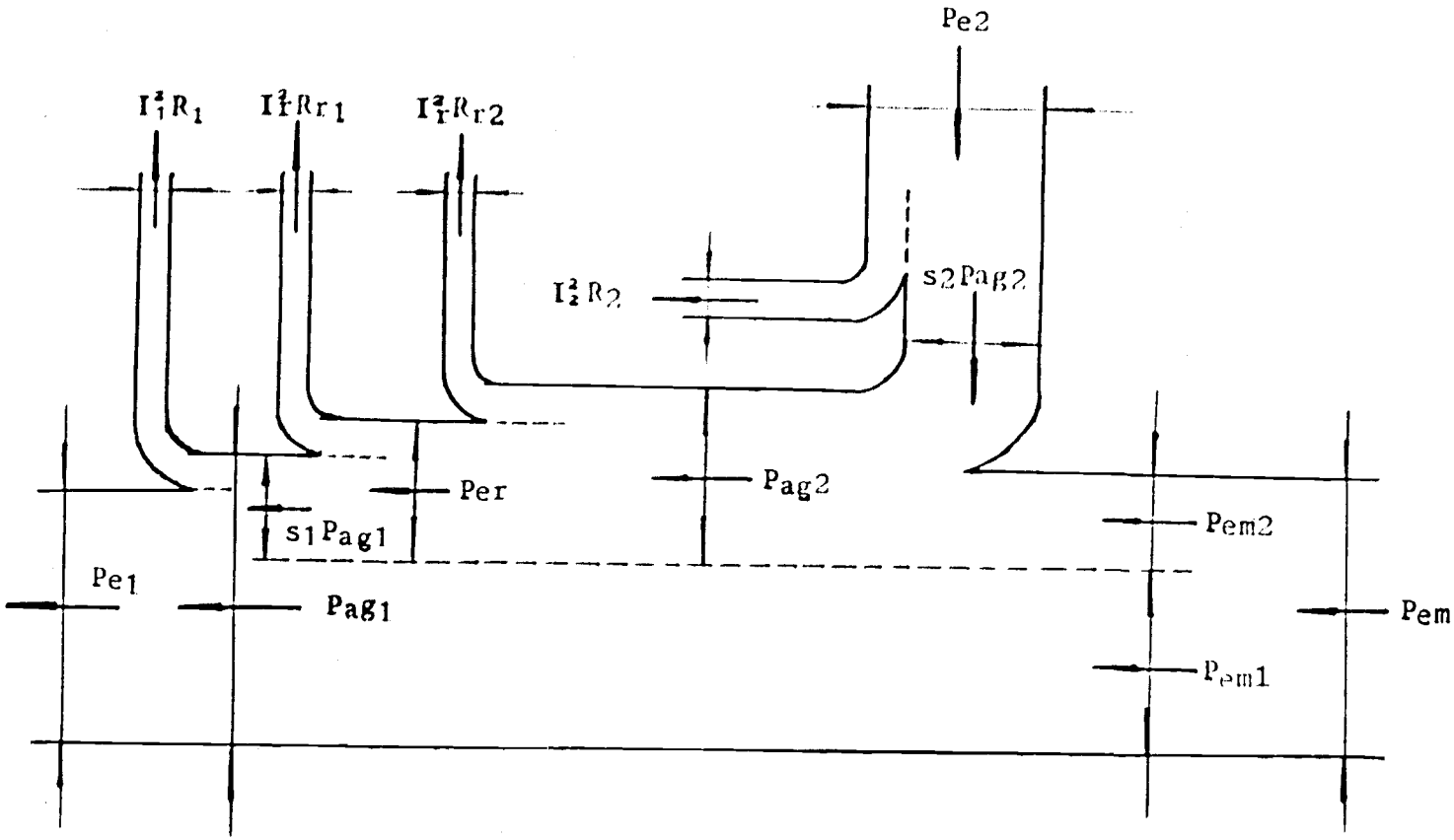

Fig.2.7 Power balance within the BDFM

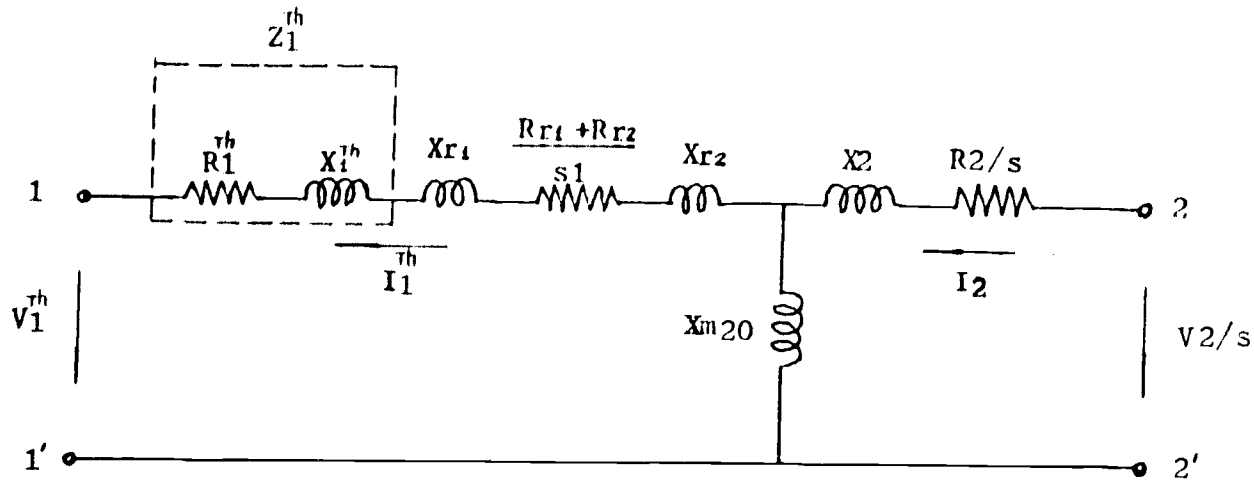

Fig.2.8 Thevenin's equivalent circuit

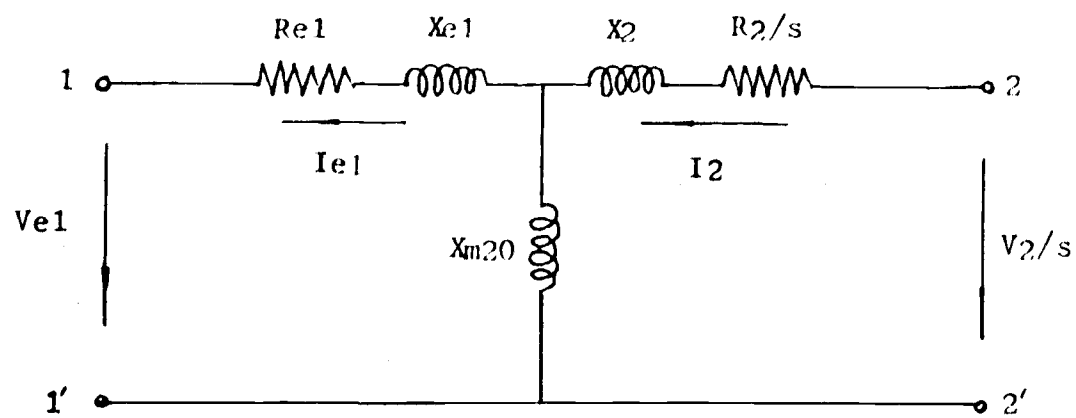

Fig.2.9 Simplified equivalent circuit of the BDFM

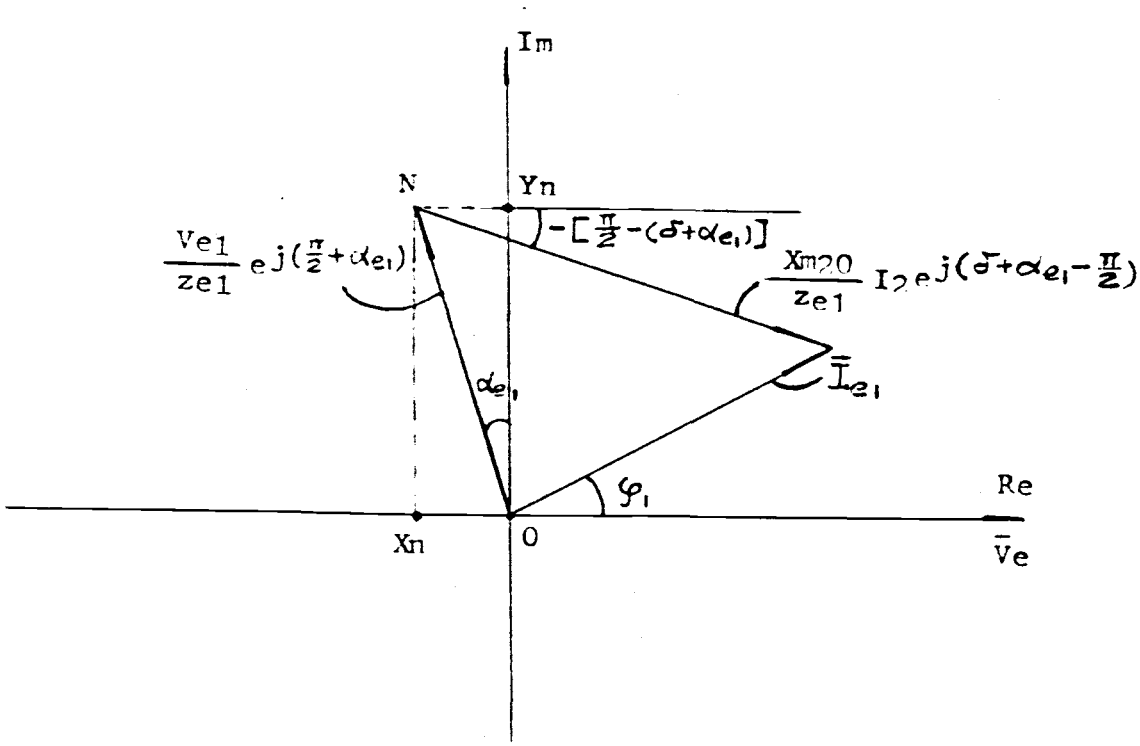

Fig.2.10 Current phasor diagram of the BDFM

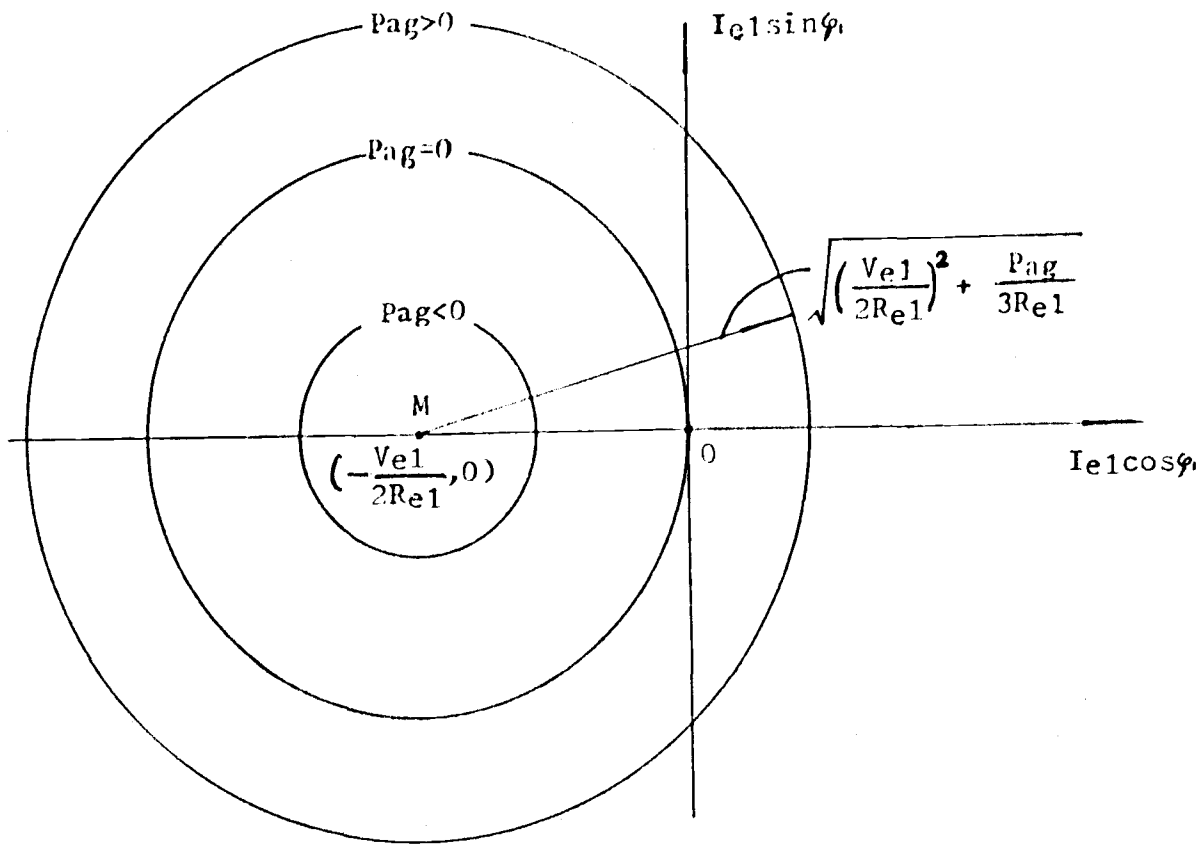

Fig.2.11 Trajectory of current I_{e1} for different P_{ag}

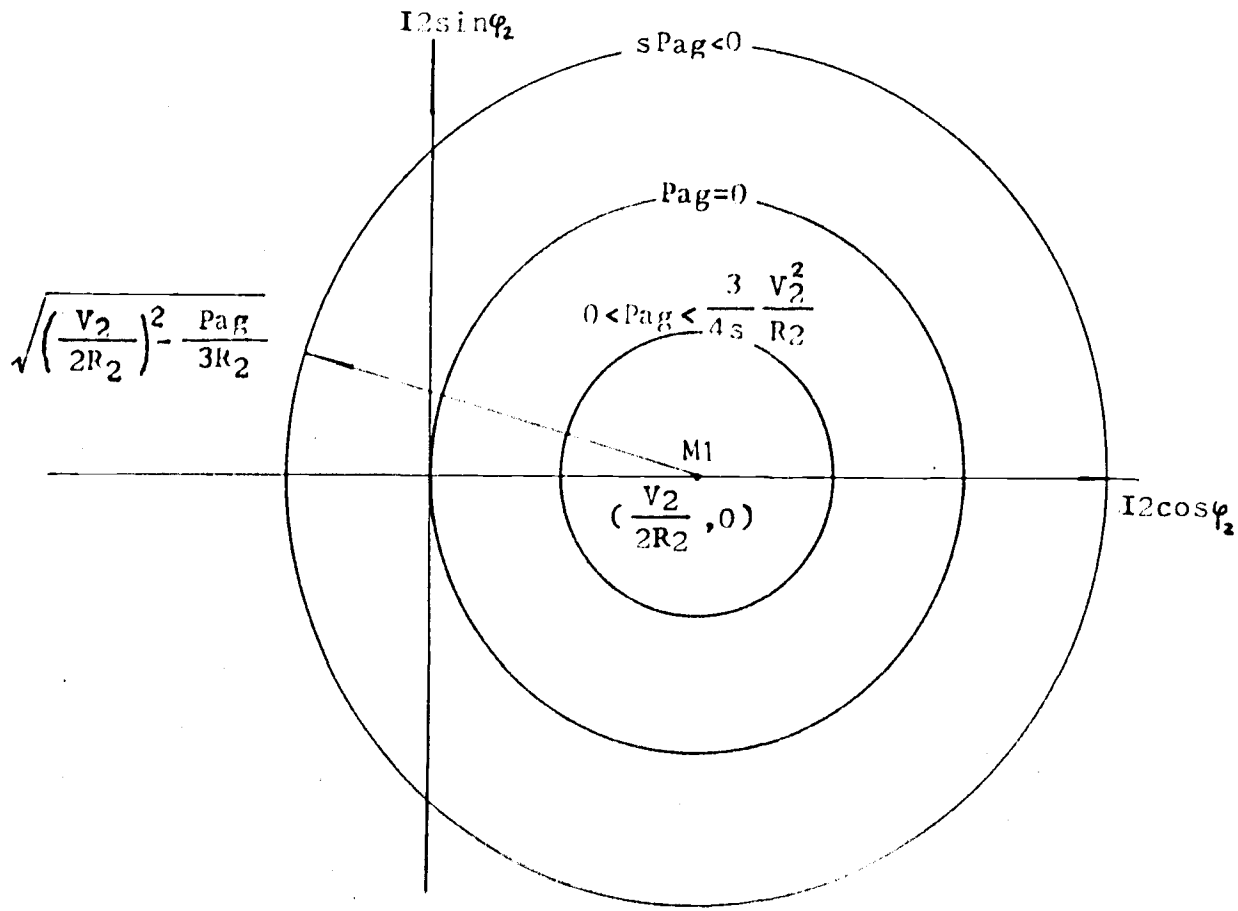

Fig.2.12 Trajectory of current I_2 for different P_{ag}

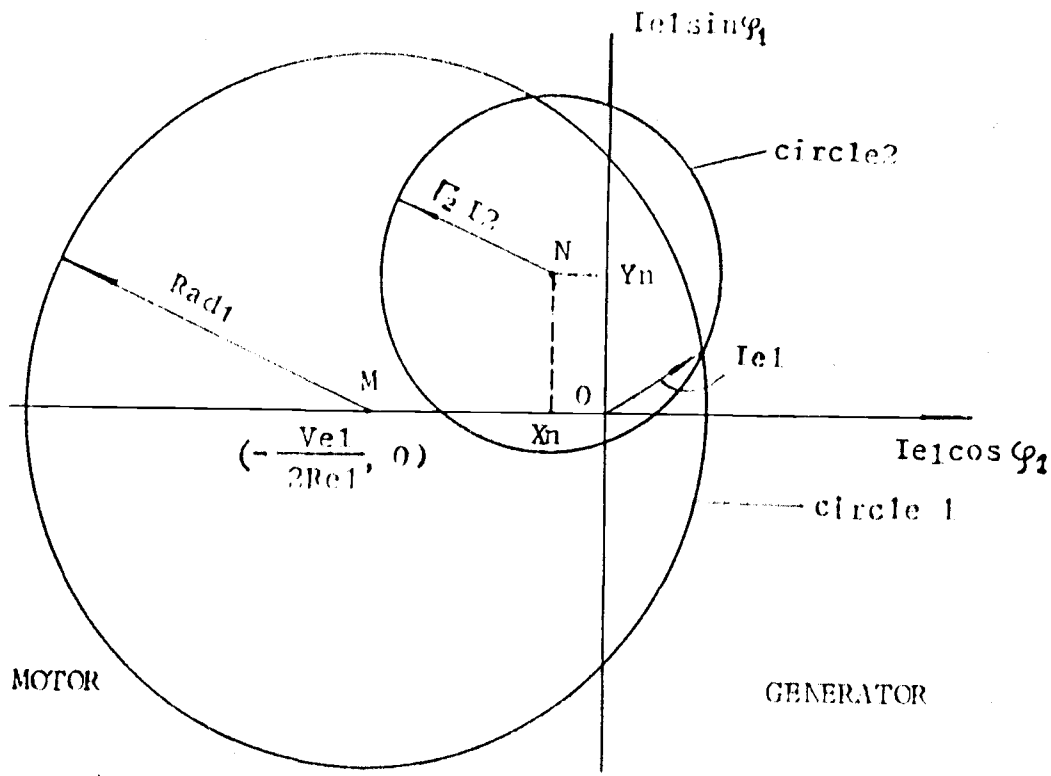

Fig.2.13 Determining the operating points of the BDFM

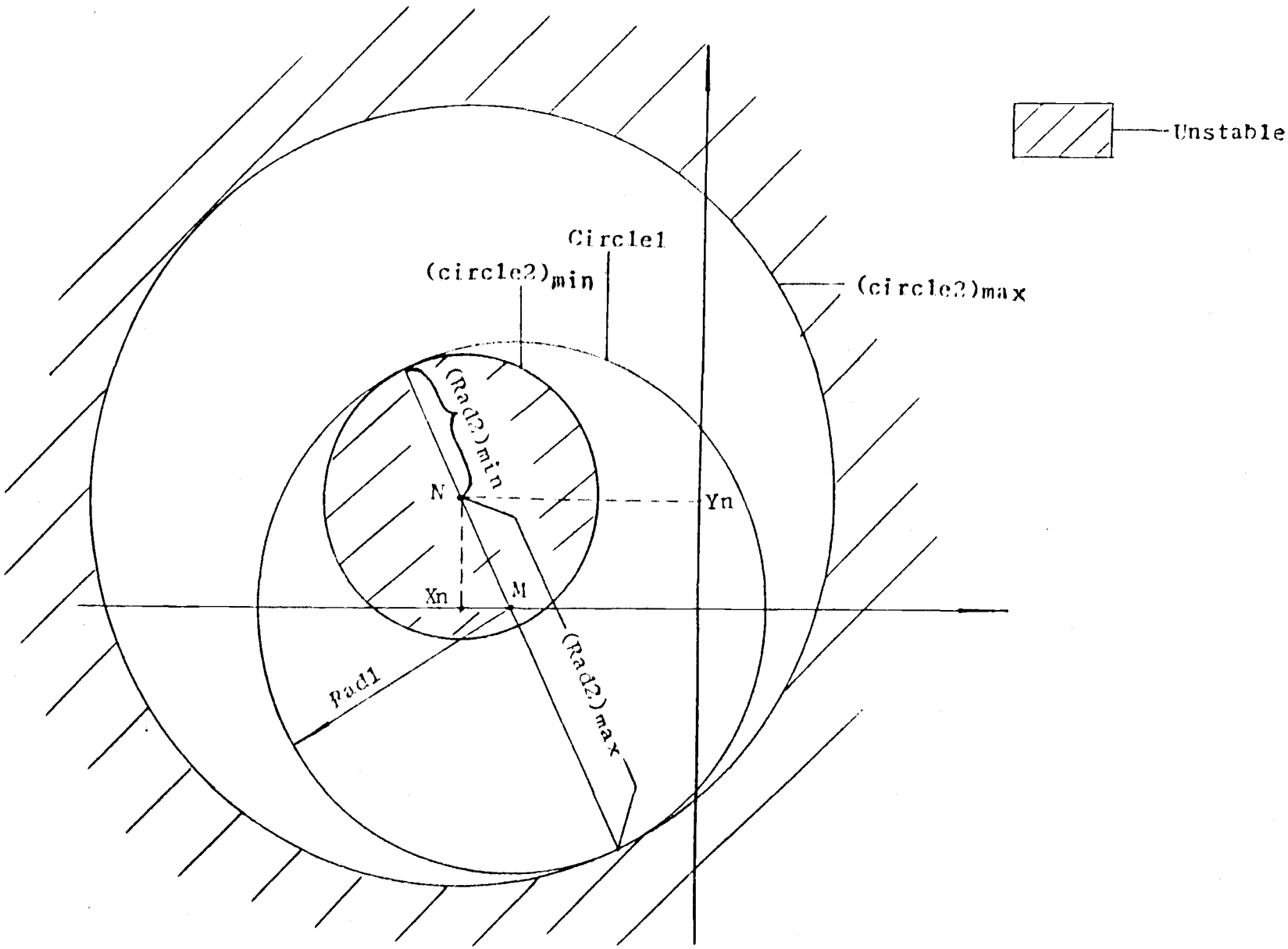

Fig.2.14 Determining the I_{2min} and the I_{2max}

3. MEASUREMENT OF THE TEST BDFM

The test BDFM used in our laboratory was a 15 KW, single-frame, single winding cascade machine. The first machine had 6 poles and the second had 2 poles. In order to analyze and predict its steady-state operating characteristics, and further, to develop these characteristics into efficient supervisory control logic to assure desired operation, the parameters of the test BDFM must be measured. The following is the measuring procedure:

Step 1: Measure R_{Aa} , the resistance between the 6-pole terminal A and the 2-pole terminal a , without either running or exciting the machine as shown in Fig.3.1. Then

$R_1 = R_2 = R_{Aa}/3$.

Step 2: Run the machine at RPM=1200 r/min. Excite the 6-pole terminals with 60 HZ and open the 2-pole terminals.Measure the values of V_1 and I_1, the voltage and current of 6-pole terminals.

Note that RPM=1200 r/min means $s_1=0$. In this case, the single-phase equivalent diagram Fig.2.5

becomes Fig.3.2. The parameters ($X_1 + X_{m10}$) will be known .

Step 3: Run the machine at RPM=1200 r/min. Excite the 2-pole terminals with 20 Hz and open the 6-pole terminals. Measure the values of V_2 and I_2, the voltage and current of 2-pole terminals.

Note that RPM=1200 r/min means $s_1=0$, and the reactance at 60 Hz equals the reactance at 20 Hz times 3. In this case the single-phase equivalent diagram Fig.2.5 becomes Fig.3.3. The parameters (X_2+X_{m20}) will be known.

Step 4: Keep the machine at standstill (i.e. $s_1=1$). Excite the 6-pole terminals with 60 Hz and short the 2-pole terminals. Measure the values of current I_1, the active power P_1 and the reactive power Q_1 in 6-pole terminals.

Because measuring X_{m10} and X_{m20} is difficult, we assume:

$$X_1 = X_{r1} = cX_{m10} \quad \text{.....(23)}$$

$$X_2 = X_{r2} = cX_{m20} \quad \text{.....(24)}$$

Usually the leakage will not more than 10%, so c μ0.1 .

In this case the single-phase equivalent diagram Fig.2.5 becomes Fig.3.4. Because X_{m10} >> $(X_{r1}+X_{r2}+R_{r1}+R_{r2})$ and X_{m20} >> (R_2+X_2), the circuit as shown in Fig.3.4 can approximately be simplified to the circuit as shown in Fig.3.5.

From Fig.3.5,

$$I_1 = I_2 ,$$

$$P_1 = I_1^2 (R_1+R_2+R_{r1}+R_{r2}) .$$

Then, $(R_{r1}+R_{r2})$ will be known.

Also, $$Q_1 = I_1^2 (X_1+X_2+X_{r1}+X_{r2})$$

thus (X_1+X_2) will be known.

According to the assumptions (23) and (24),

$$(X_1+X_2)/\{(X_{m10}+X_1)+(X_{m20}+X_2)\}=c/(1+c)$$

c will be known, hence the parameters $X_1, X_2, X_{r1}, X_{r2}, X_{m10}, X_{m20}$ will be known.

The results of the measurement are:

step 1: R_{Aa}= 3.4 ohm ,

step 2: V_1 = 106.38 v (V_1 is the line voltage),

I_1 = 1.72 a ,

step 3: V_2 = 68.8 v (V_2 is the line voltage),

I_2 = 5.0 a ,

step 4: (1) P_1 = 764 w, I_1 = 7.21 a ,

(2) Q_1 = 1170.9 w, I_1 = 7.35 a .

The results of the measurement give the parameters of the test BDFM as following:

$R_1 = R_2$ = 1.133 ohm ,

$R_{r1} + R_{r2}$ = 2.63 ohm ,

X_1+X_{m10} = 35.69 ohm ,

X_2+X_{m20} = 23.59 ohm ,

c = 0.065 ,

$X_1 = X_{r1}$ = 2.18 ohm ,

$X_2 = X_{r2}$ = 1.44 ohm ,

X_{m10} = 33.51 ohm ,

X_{m20} = 22.15 ohm .

4. RESULTS AND VERIFICATION

According to the measured parameters the analysis of the steady-state performance of the test BDFM was made by means of a HP-1000 computer. All plots were plotted with the HP-9872B plotter. In the following sections the main results are described.

4.1 EFFECT OF SPEED ON PARAMETERS OF THE BDFM

For convenience and convention sake, the conventional machine parameters are used to describe the BDFM and to analyze its performance. For the conventional doubly-fed machine, all its parameters are constant and don't depend on the speed of machine. However, for the BDFM some its parameters depend on the speed of machine. This is the important difference between the conventional doubly-fed machine and the BDFM. From the equivalent circuit of the BDFM, as shown in Fig.2.9, it is noted that the parameters R_{e1} and Z_{e1} are not constant, they depend on the speed, or the slip s. It is hard to analyze these parameters. But, the use of the computer analysis is easy to get the tendency of parameters with the speed.

Fig.4.1 to Fig.4.5 show the computer analysis results which described the effect of the speed on some parameters.

Fig.4.1, Fig.4.2 and Fig.4.3 show the curves of parameters R_{e1}, X_{e1} and Z_{e1} versus the slip s for our test BDFM. It can be observed from Fig.4.1 and Fig.4.2 that the parameters R_{e1} and Z_{e1} are not constant at all. They have a jump at s=-0.333, which means that the test machine can not be operated at this speed. We must avoid this speed in its operation. Fortunately, in the normal operating regions (from s=0 to s=1) the effect of the speed on R_{e1} and Z_{e1} is small, as shown in Fig.4.3, i.e. R_{e1} and Z_{e1} are almost constant like a conventional doubly-fed machine. From a operational point of view, it is desirable to have the parameters of the BDFM to be close to constants. Therefore, when designing the BDFM some adjustment of certain parameters may be necessary. If the effect of the slip on R_{e1} is too high, appropriate increase of R_1 and X_{m10}, or appropriate decrease of $(R_{r1} + R_{r2})$ can make R_{e1} close to a constant.

Fig.4.4 shows the curve of the coefficient $\tilde{a}_2$ versus the slip s. As mentioned in section 2.2.3, $\tilde{a}_2$ is not constant for the BDFM. However, if R_{e1} remains constant practically, then $\tilde{a}_2$ will also be a constant.

Fig.4.5 shows the effect of speed on the location of points N and M. For the conventional doubly-fed machine the points N and M are fixed. For the BDFM, however, they vary with the slip s. This is because R_{e1} is not a constant for the BDFM, it depends on the slip s. From the point of view of operation, it is highly desirable to have the location of points N and M to be independent of the slip s. Consequently, R_{e1} should be designed to be close to a constant.

4.2 EFFECT OF DIFFERENT MECHANICAL INPUT CONDITIONS

Analyzing operating characteristics of the BDFM under different mechanical input conditions is one of our objectives in this thesis. Fig.4.6 to Fig.4.9 show different input mechanical characteristics (the power-speed characteristic). Fig.4.6, Fig.4.7 and Fig.4.8 show the light-load cubic characteristic, light-load constant characteristic and light-load linear characteristic respectively. These three curves represent the situations for which practically no mechanical power is provided to the BDFM. It is basically the effect of damping torque that is being considered. Fig.4.9 shows the full-load cubic characteristic. This is a typical power-speed characteristic of hydro or wind turbines.

Fig.4.10 to Fig.4.13 show the effect of the considered mechanical input characteristics on the stability of the operating modes. These results clearly indicated that stability can only be maintained if the exciting current is within certain limits (I_{2max} and I_{2min}). These limits are dependent on the speed. If the "exciting current" I_2 is beyond these limits, the BDFM will loose the synchronous mode and will exhibit the asynchronous (induction) mode of operation. This conclusion was confirmed by the observations made of the performance of the designed BDFM . Thus, for stable synchronous operation of the BDFM the "exciting current" I_2 must be controlled to assure values between I_{2max} and I_{2min}.

Fig.4.14 to Fig.4.17 show the effect of different mechanical input characteristics on the trajectories of the operating points. As mentioned in section 2.2.3, the trajectory of operating points I_{e1} at a specified speed is a circle with the center M and radius OM. At different speeds the circles are different. For different mechanical input characteristics the trajectories of operating points I_{e1} are different too. Fig.4.14, Fig.4.15 and Fig.4.16 correspond to input 1,2 and 3 respectively. Under these circumstances no mechanical input power other than damping power is

supplied to the machine. The results show that all these circles are on the left half plane. This means that the BDFM operates in the motor mode.

Fig.4.17 corresponds with input4 (the full-load cubic characteristic). Under this circumstance the BDFM may operate in the generator mode .

4.3 EFFECT OF DIFFERENT X_{m20} PARAMETERS

Some parameters are quite important to the operation of the BDFM. X_{m20} is certainly one of these parameters.

Fig.4.18 shows the effect of different X_{m20} on the positions of points N and M. From this plot it is clear that the higher the parameter X_{m20} , the less the locations of points N and M change.

Fig.4.19, Fig.4.20, Fig.4.21 and Fig.4.22 show the effect of different X_{m20} on the stability. These plots indicate that if X_{m20} is too small, then I_{2min} and I_{2max} will be very high as shown in Fig.4.19. This will cause the machine rating to be too high. This phenomenon was observed in our laboratory VSG system. In measurements it was found that when X_{m20} of our test BDFM is small (in our first design, X_{m20} is 0.6 ohm),

the BDFM could not be pulled into synchronizm at V_1=115v. An excessively high voltage would be required to provide the high excitation current, as can be concluded from the plot results. After redesigning the BDFM, the parameter X_{m20} was increased to 22.15 ohm which allows the BDFM to be locked into synchronizm at V1=115v. This means that I_{2min} is lower when X_{m20} is higher. This was predicted by the theory and shown in Fig.4.19. Fig.4.20, Fig.4.21 and Fig.4.22 show the stability limits for X_{m20}=1.0 ohm, 10.0 ohm and 30.0 ohm respectively. These results explain and verify the phenomenon observed in our labolatory VSG system. In conclusion, the BDFM should not be designed with the parameter X_{m20} too small.

4.4 EFFECT OF DIFFERENT R_r PARAMETERS

Another important parameter to the operation of the BDFM is the rotor resistance (assume R_{r1}=R_{r2}).

Fig.4.23 is the result of the computer analysis. It indicates that if R_r is too high, then I_{2min} and I_{2max} are close to each other at s=0, i.e. the excitation current is required to be controlled within tight limits to assure stability at s=0. Therefore, the rotor of the BDFM should be designed to have minimal resistance R_r in order to assure stable operating

conditions with a satisfactory excitation current margin.

4.5 DETERMINE EXCITING CURRENTS I_2 AT ZERO REACTIVE POWER OUTPUT FOR DIFFERENT INPUT CHARACTERISTICS

The controller of the VSG system set up in our laboratory was provided with a reactive power controller which was verified to be capable of securing steady-state stability. Controlling the reactive power output rather than the torque angle is obviously more convenient from the data acquisition point of view. The effectiveness of the reactive power controller in securing steady-state stable operation can be predicted from the circle diagram. If the reactive power output controller maintains operation on the horizontal axis, zero reactive power output (P.F.=1) is allowed. For a given input power-speed characteristic the curves of the required excitating currents I_2 versus the slip for zero reactive power output (i.e. P.F.=1) can be easily predicted on the basis of the circle diagram method.

Fig.4.24 to Fig.4.27 are results which show the curves of the required exciting currents I_2 versus the slip s at zero reactive power output for different input characteristics. Maintaining these required exciting currents can prevent operation beyond the

steady-state stability limit. The underlying relationships of the circle diagram method can be developed into efficient supervisory control logic to assure desired operation under varying resource conditions.

4.6 VERIFICATION

Due to time constraints, no exhaustive measurements could be taken in order to verify results obtained from the computer analysis. However, the theory developed and the analysis presented in this thesis were qualitatively completely confirmed by the observations conducted on the designed BDFM, as was mentioned in section 4.2, 4.3 and 4.4.

The theory presented in this thesis presents a means to analyze the tendency of the operating conditions of the BDFM when some conditions are changed. The performance of the BDFM observed in our laboratory system has verified our theory. Moreover, this theory was used to improve some parameters of the BDFM in order to obtain the desired performance as described in section 4.3. Further study to obtain more accurate results is recognized to be needed. The effect of increased rotor resistance due to skin effect and the effect of saturation are worth pursuing. A follow

up on this study should include a transient analysis which requires the development of a transient model of the BDFM.

5. CONCLUSIONS

The objective of this thesis was to study the operating characteristics of the BDFM under the doubly-fed mode (synchronous mode). The following main conclutions can be drawn:

(1) Several authors have dealt with the general analysis of the singly-fed mode (asynchronous mode) of the BDFM. But there was no paper to deal with the operating characteristics of the BDFM under the doubly-fed mode (synchronous mode). The analysis method and the steady-state operating characteristics of the BDFM under doubly-fed mode were presented in this thesis.

(2) A critical condition for stable steady-state operation in the synchronous mode is found to be formed by the exciting current I_2. This current must be controlled to stay within certain limits, i.e. between I_{2min} and I_{2max}. Finding I_{2min} and I_{2max} at any specified speed and controlling I_2 to prevent loss of synchronizm was subject of the analysis presented. It can be concluded that a zero-reactive power output control could be an effective and convenient control method. By computer analysis based on the circle diagram method the "exciting currents" I_2 at zero

reactive power output can be established. The associated computer algorithm can be developed into an efficient supervisory control logic to assure stable steady-state operation of the BDFM under varying resource conditions.

(3) Some parameters of the BDFM are not constant. They depend on the slip s. This is the crucial difference between the conventional doubly-fed machine and the BDFM. This fact must be taken into account in considering the performence of the BDFM. Detailed results in this respect were presented in chapter 4. Recommendations to minimize the adverse effects of the speed on the parameters of the BDFM were also given.

(4) The circle diagram method was demonstrated to be an effective and convenient method to analyze the operating characteristics of the BDFM. All important operating characteristics of the BDFM can be obtained based on this method, i.e. the method can successfully explain and predict the operating performance of the machine. Moreover, it can be used to improve some parameters of the BDFM in order to obtain the desired performance.

(5) Further study to obtain more accurate results is recognized to be needed. The effect of increased

rotor resistance due to skin effect and the effect of saturation are worth pursuing. A follow up on this study should include a transient analysis which requires the development of a transient model of the BDFM.

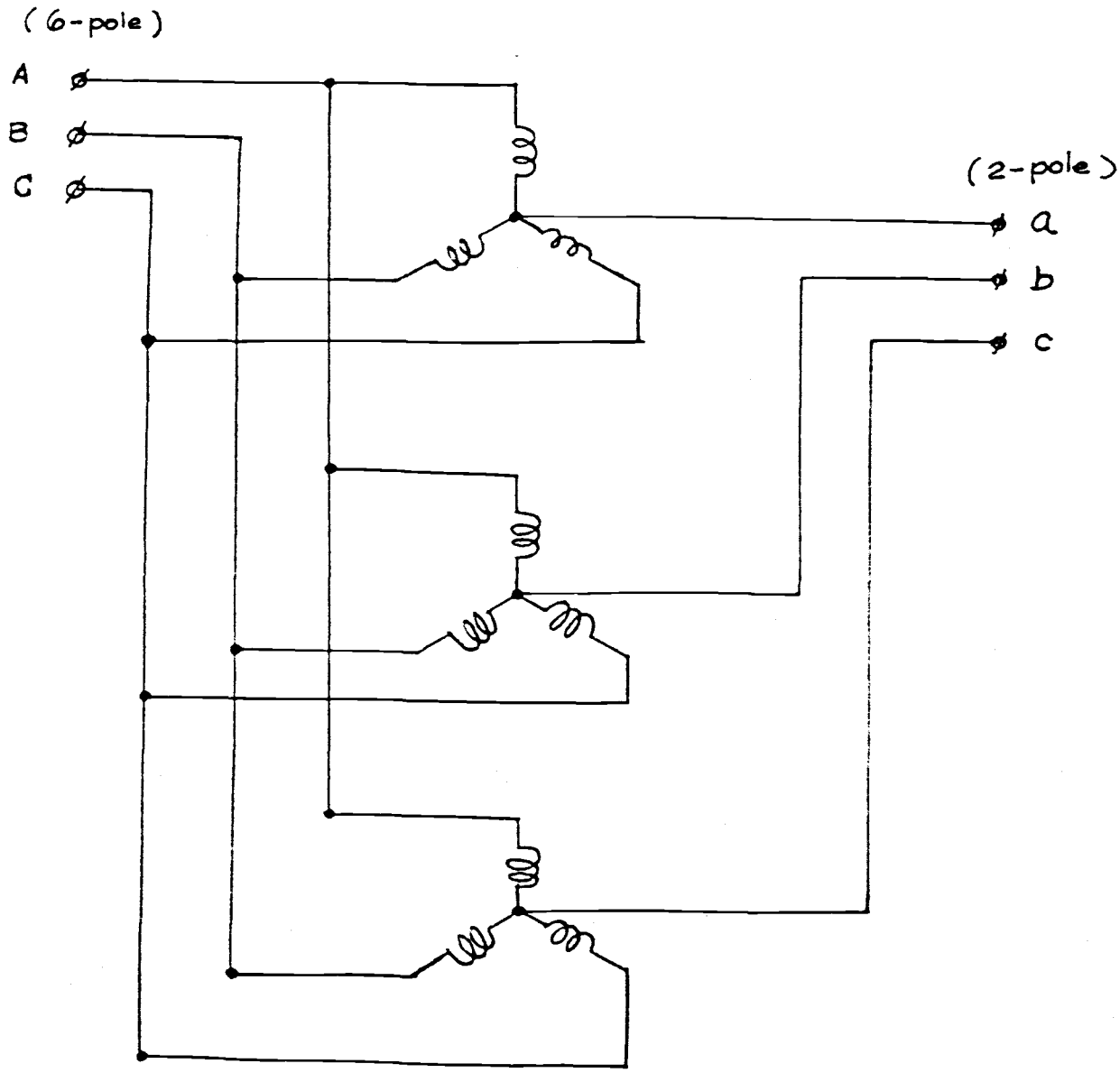

Fig.3.1 Measurement circuit for step 1

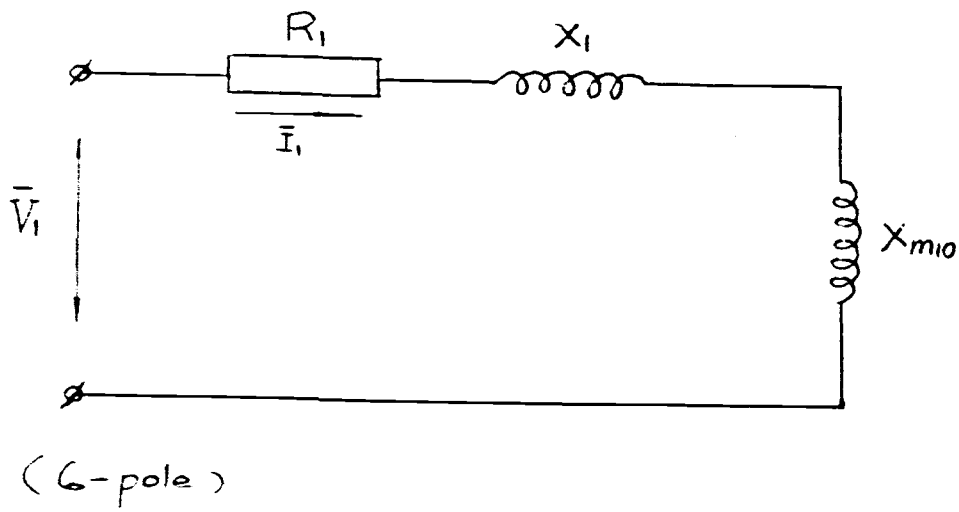

Fig.3.2 Measurement circuit for step 2

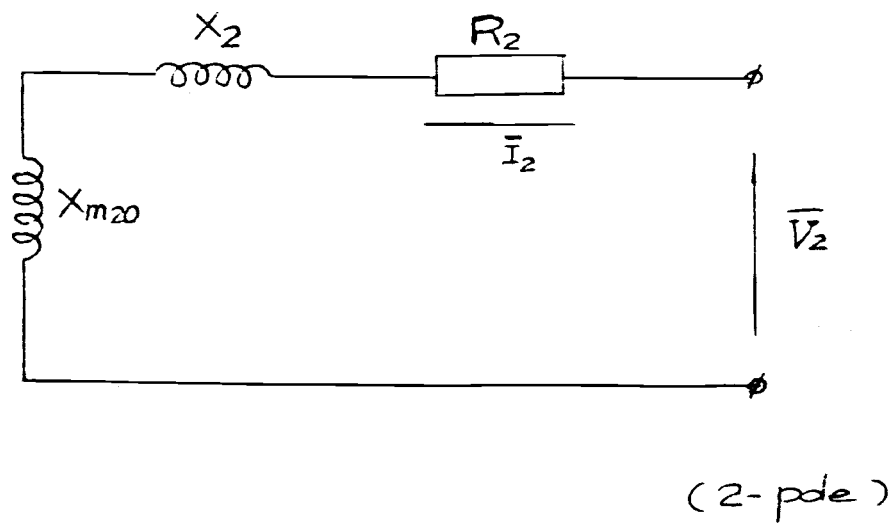

Fig.3.3 Measurement circuit for step 3

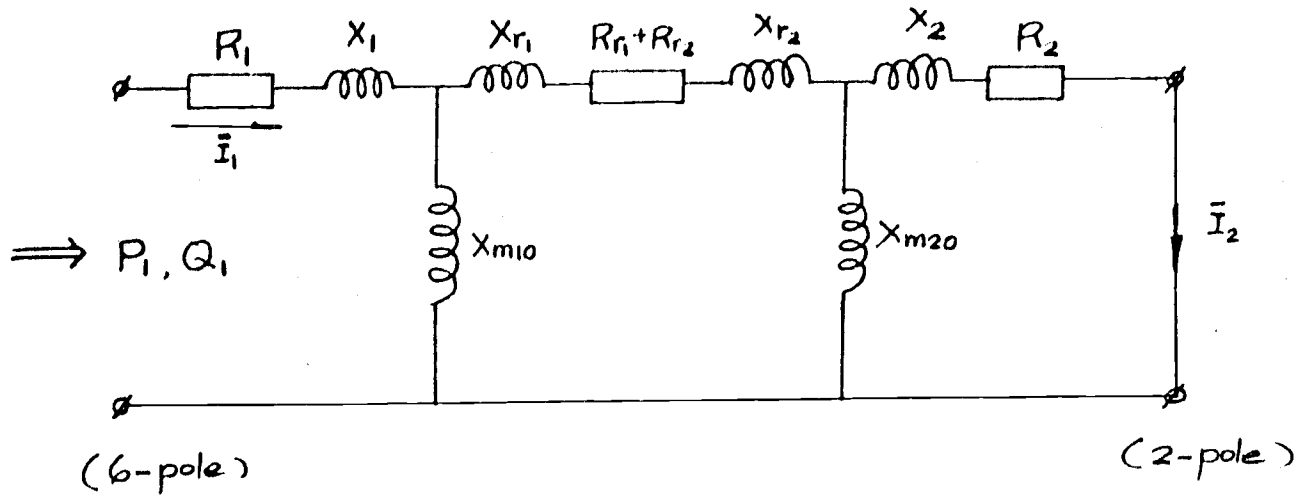

Fig.3.4 Measurement circuit for step 4

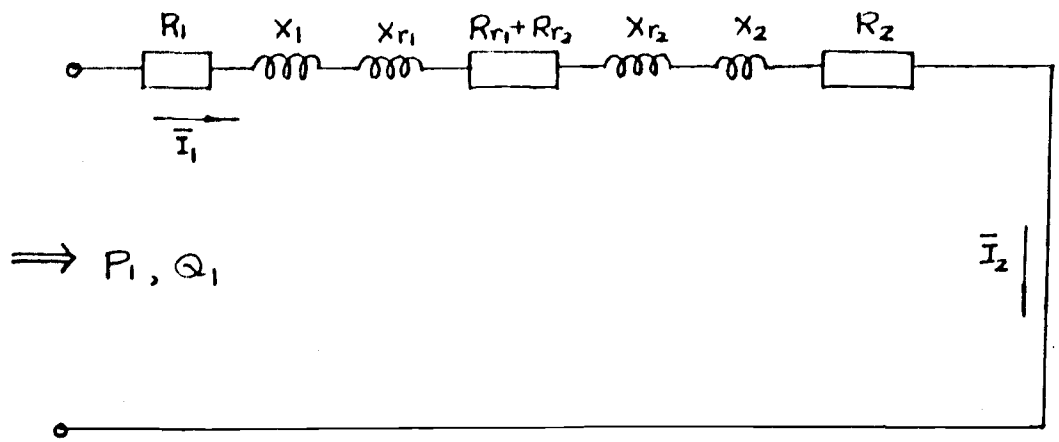

Fig.3.5 Simplified measurement circuit

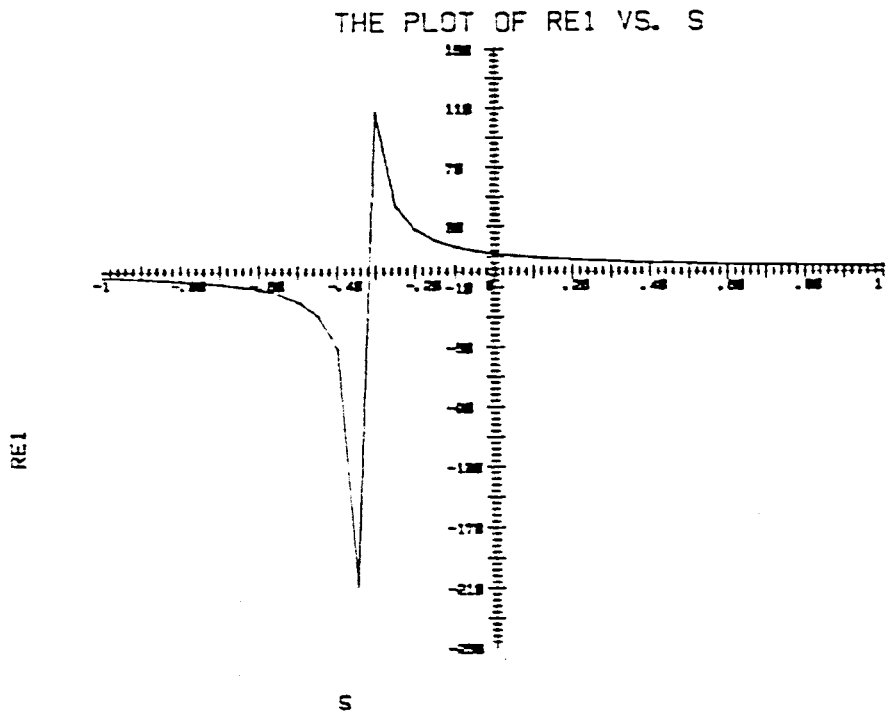

Fig.4.1 The curve of R_{e1} versus slip s

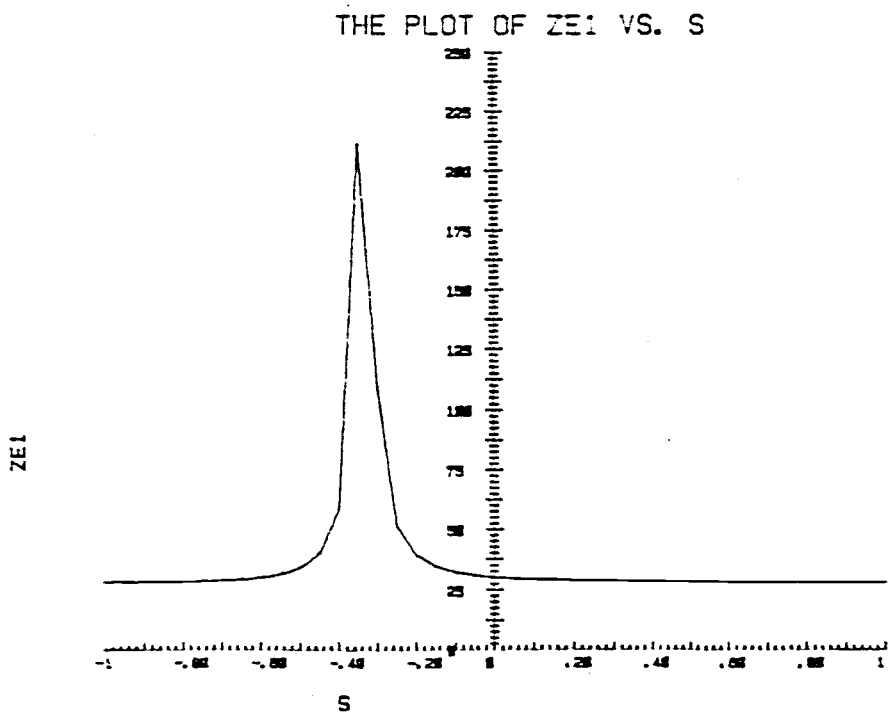

Fig.4.2 The curve of Z_{el} versus slip s

Fig.4.3 The curves of R_{e1} , X_{e1} & Z_{e1} versus slip s

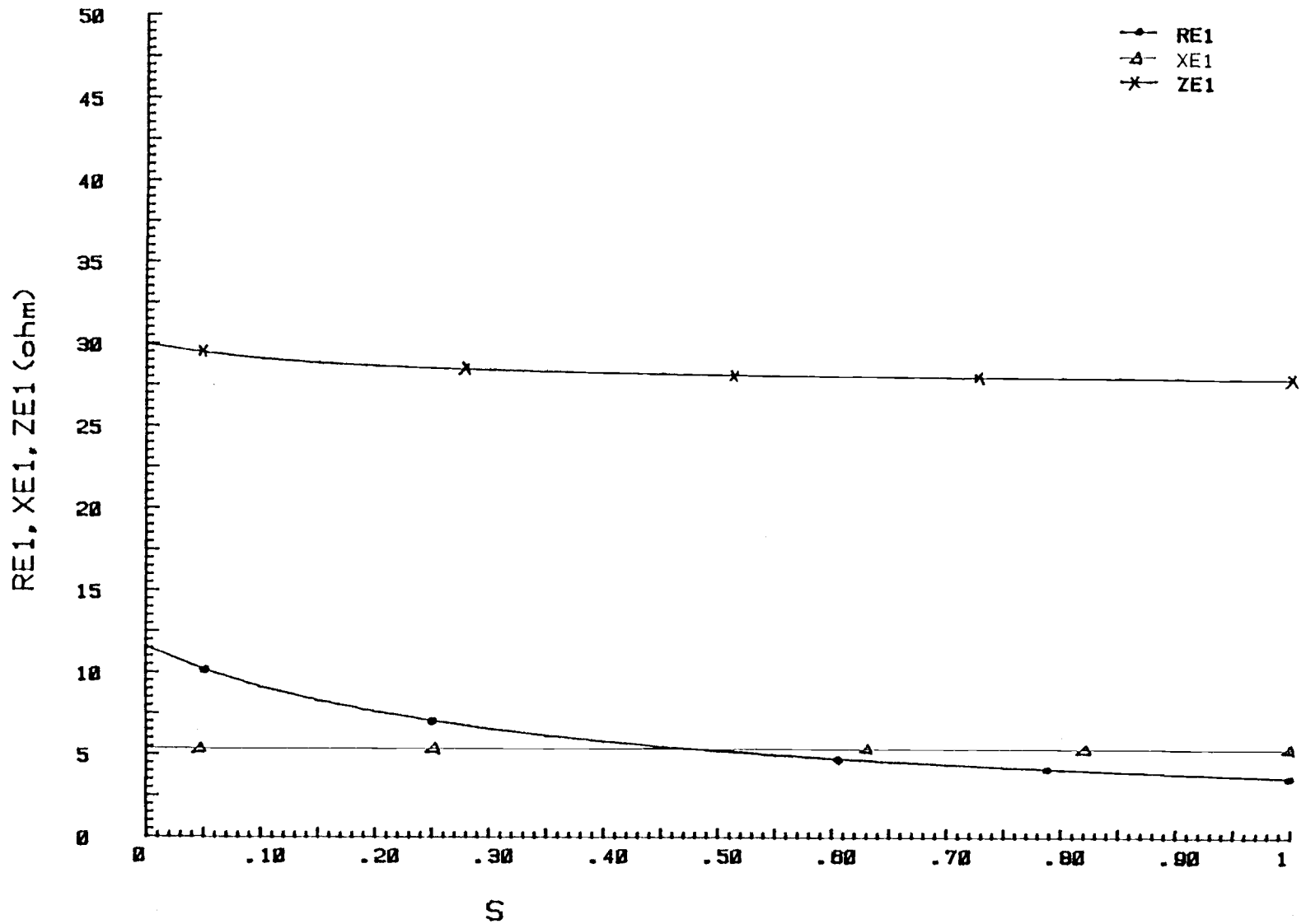

Fig.4.4 The curve of Γ_2 versus slip s

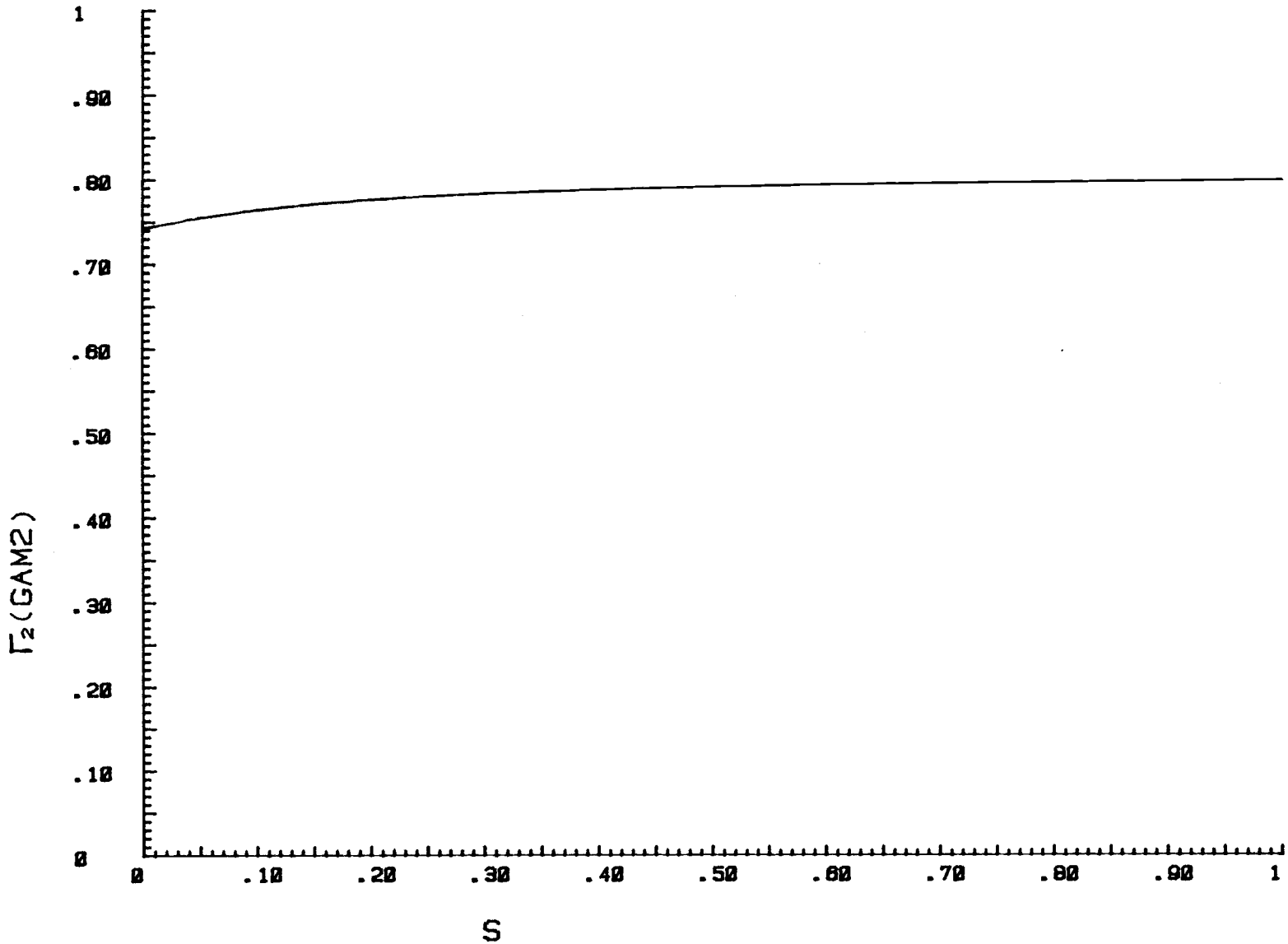

Fig.4.5 The plot of points N and M

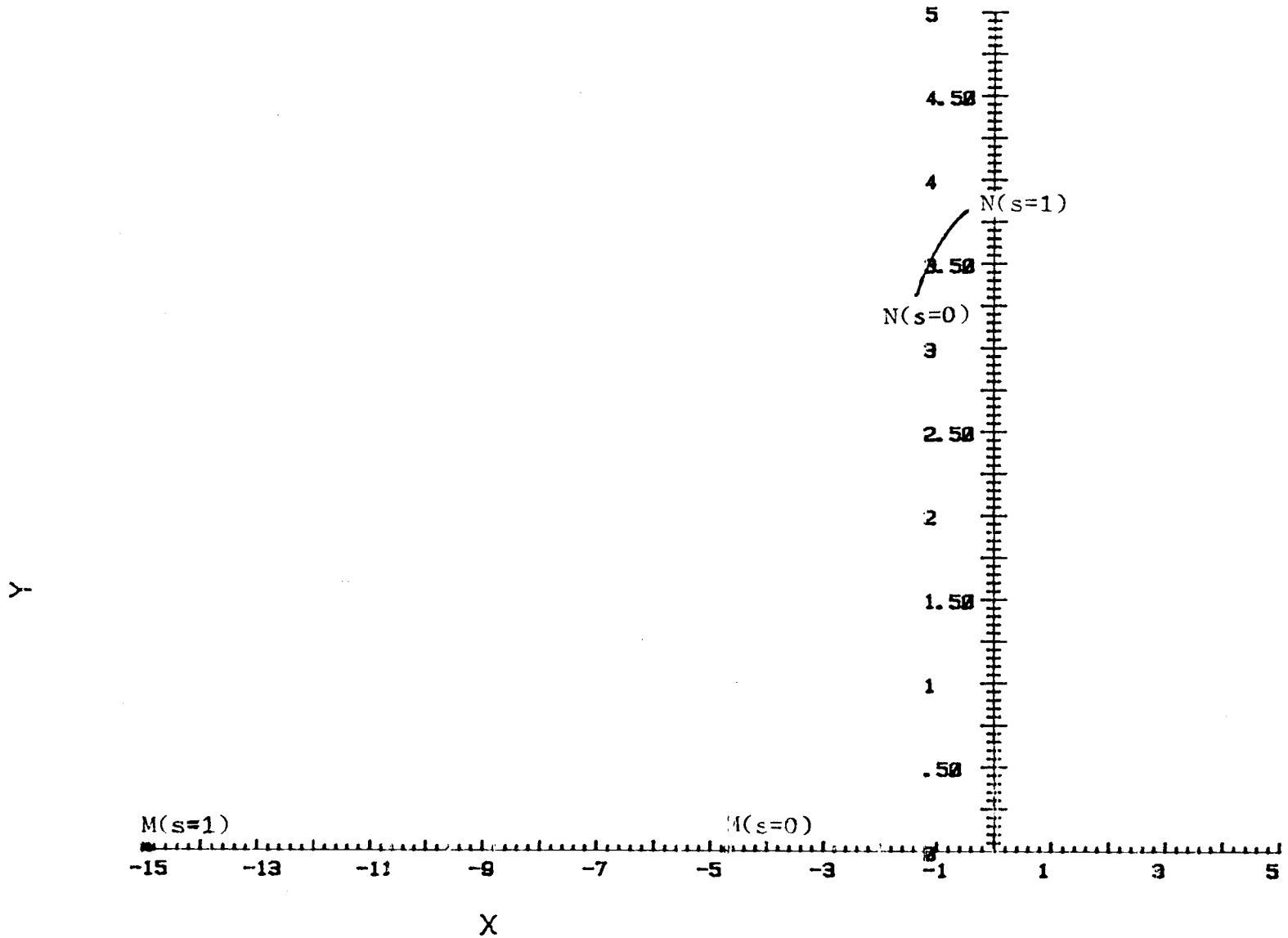

Fig.4.6 The characteristic of input 1

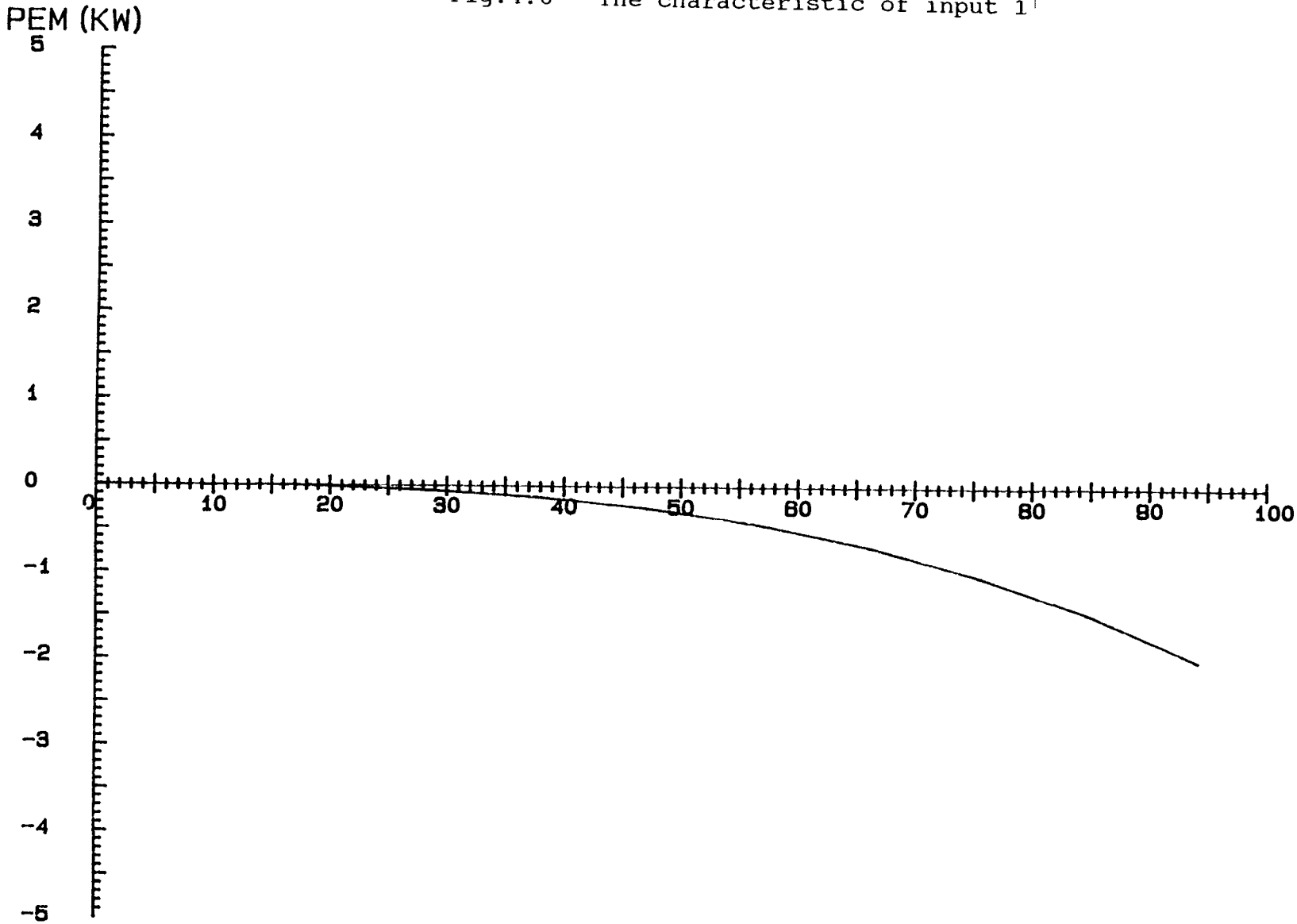

Fig.4.7 The characteristic of input 2

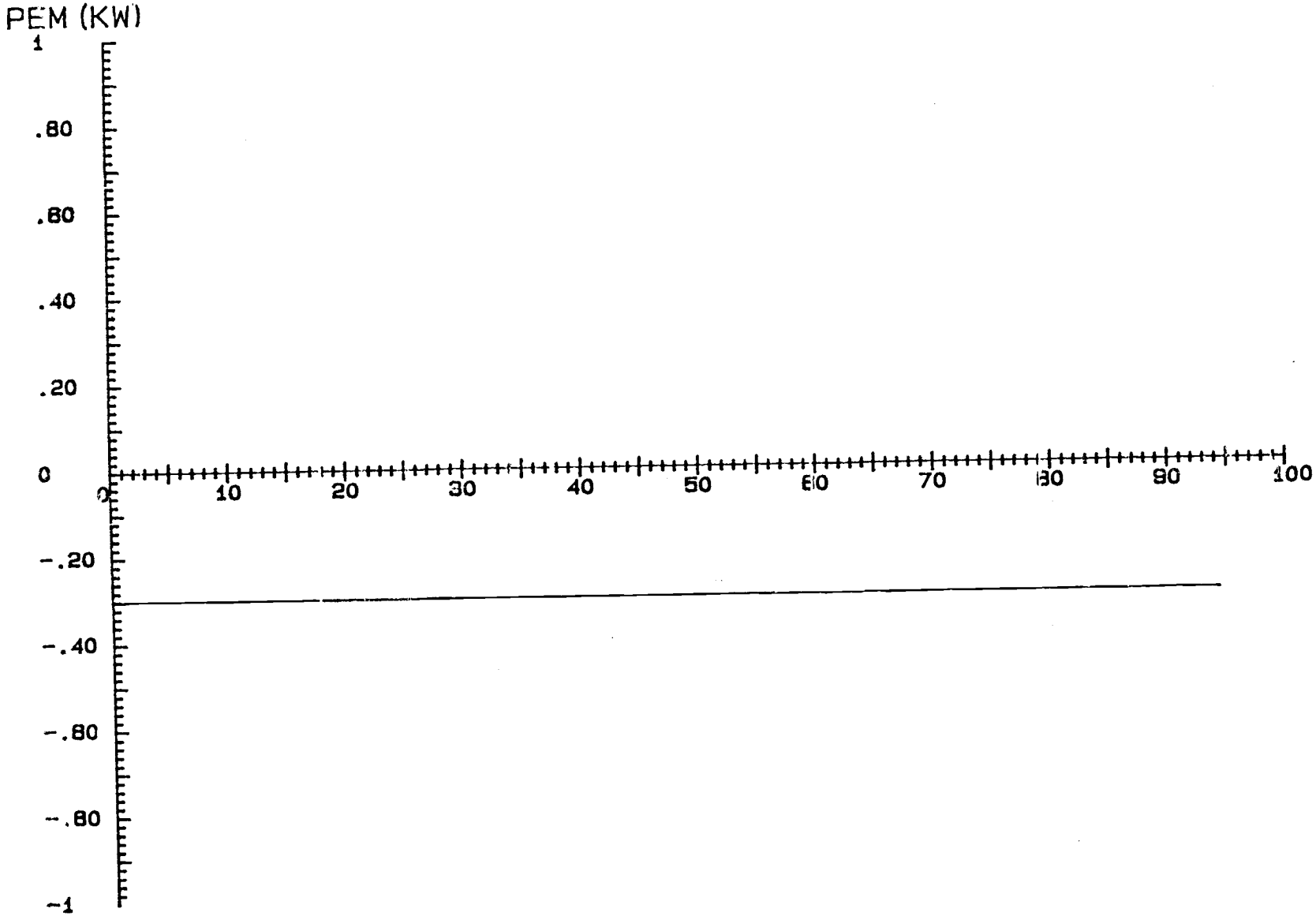

Fig.4.8 The characteristic of input 3

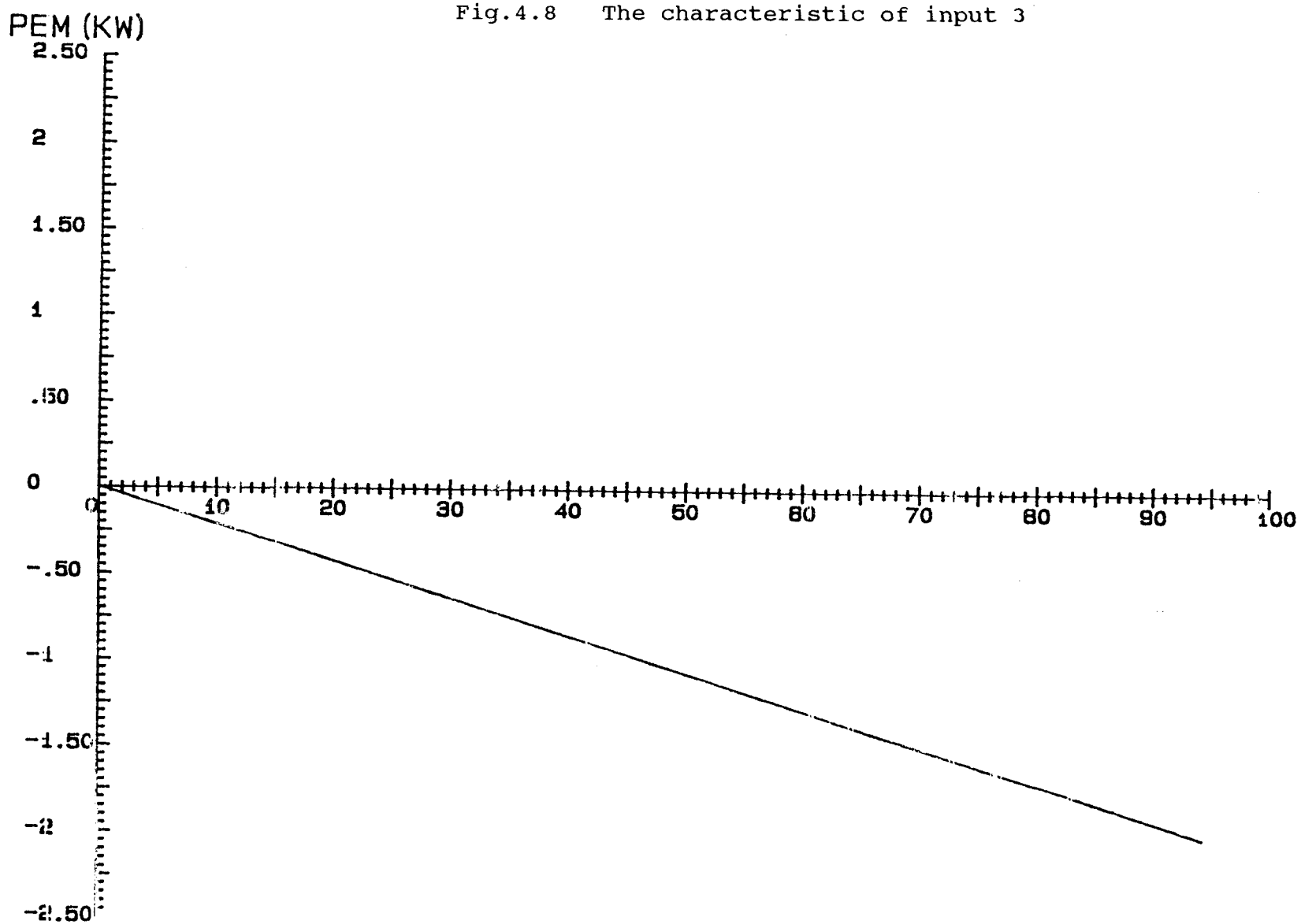

WM

Fig.4.9 The characteristic of input 4

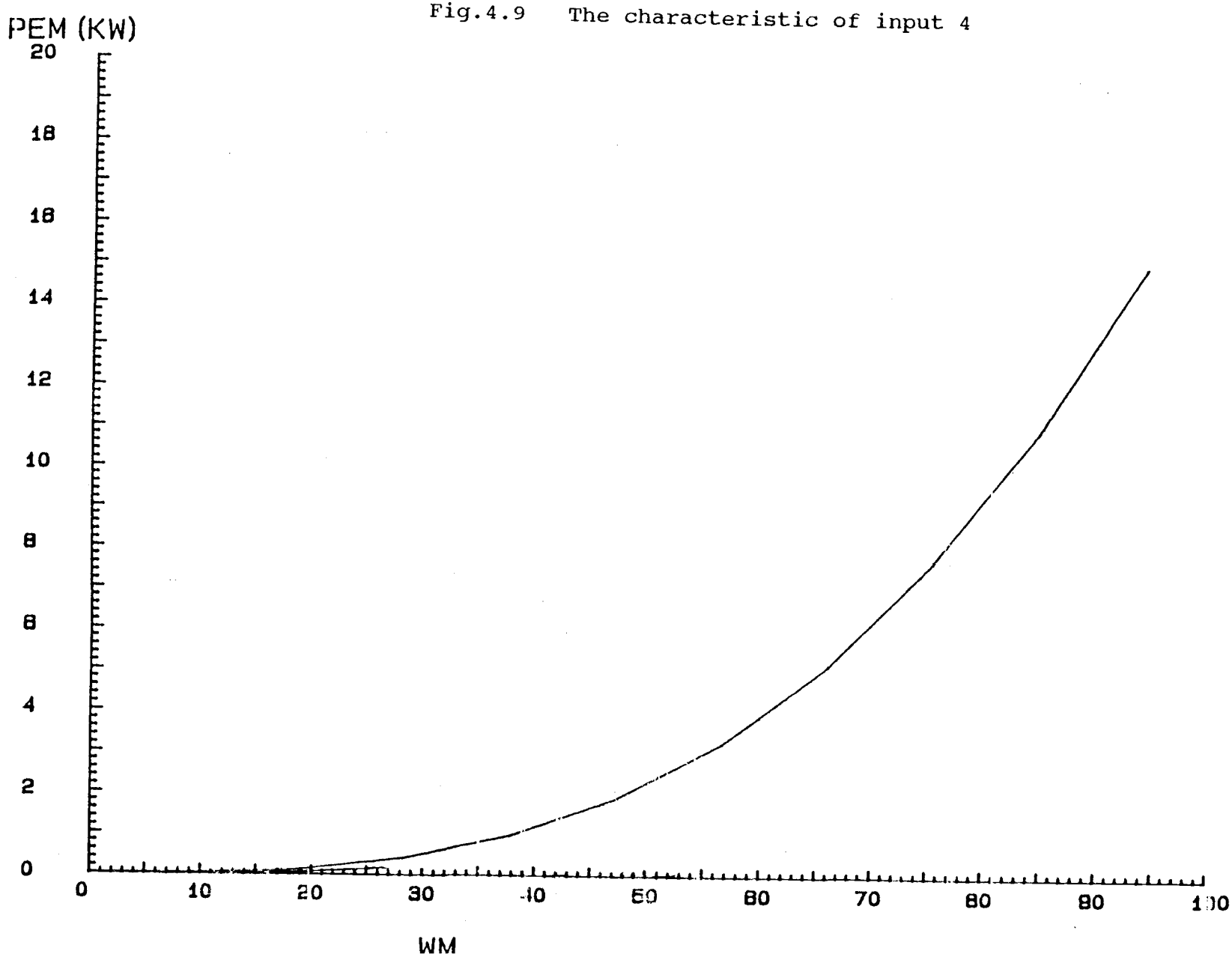

Fig.4.10 The curves of I_{2min} and I_{2max} versus slip s for input 1

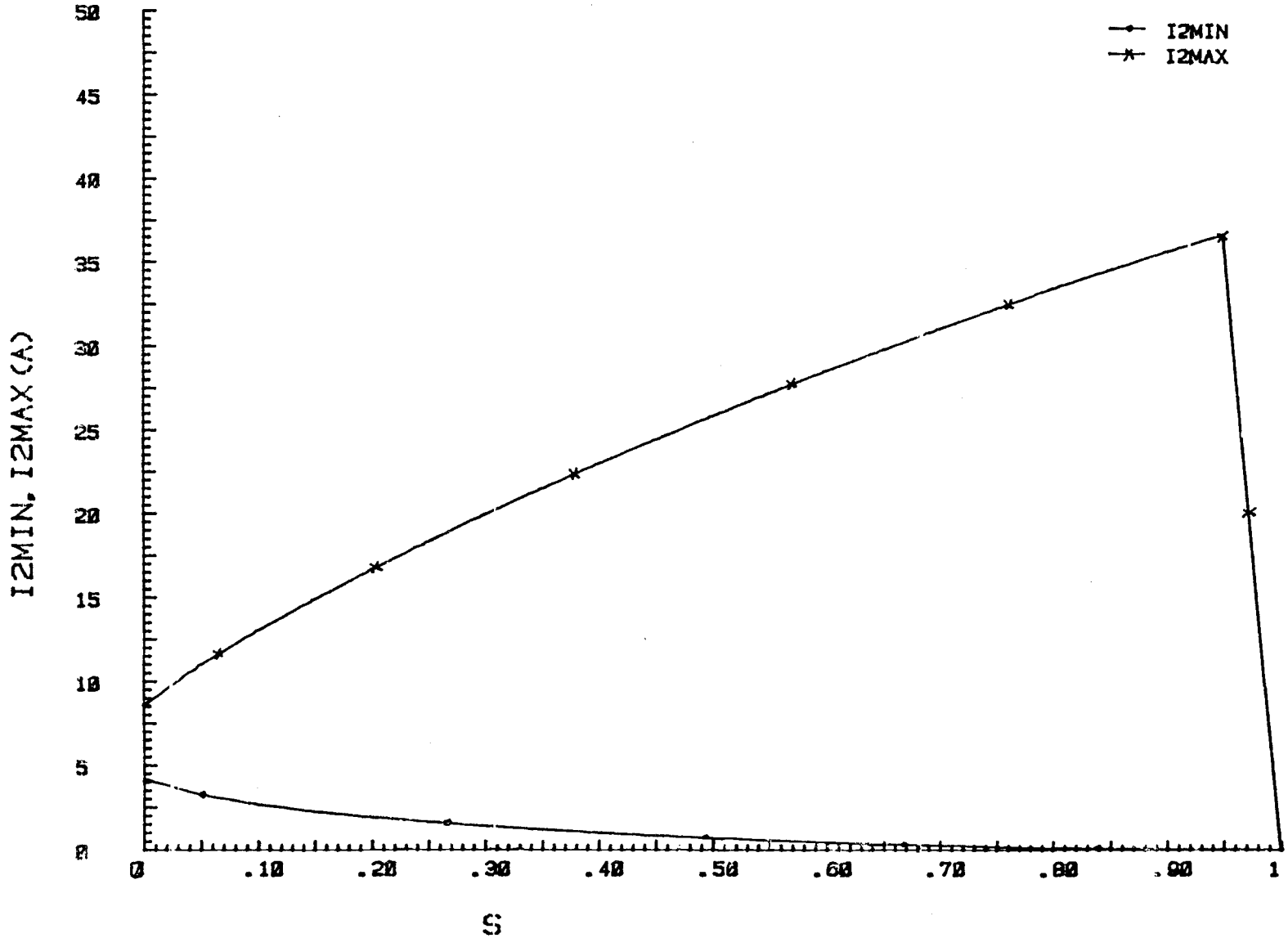

Fig.4.11 The curves of I_{2min} and I_{2max} versus slip s for input 2

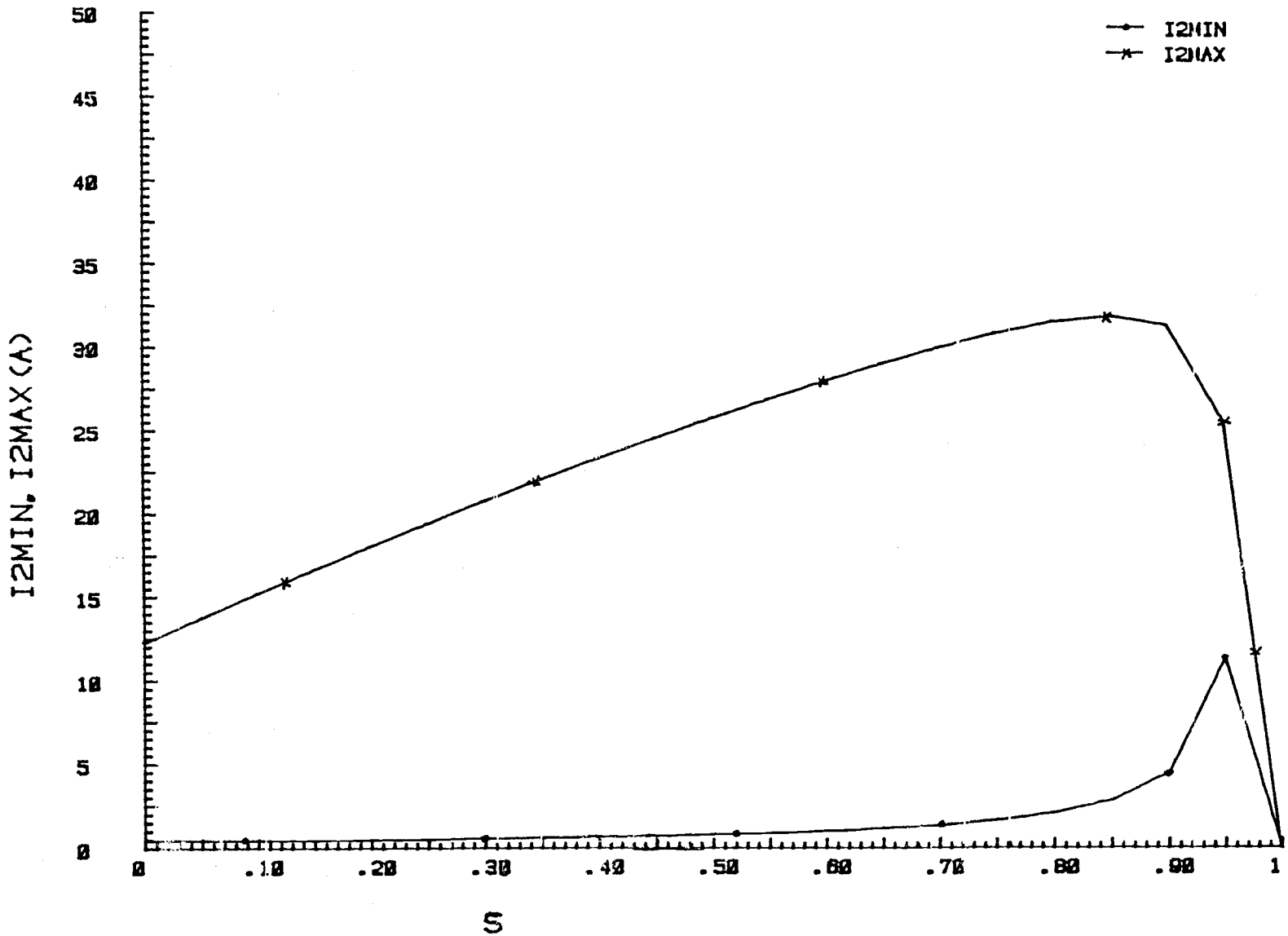

Fig.4.12 The curves of I_{2min} and I_{2max} versus slip s for input 3

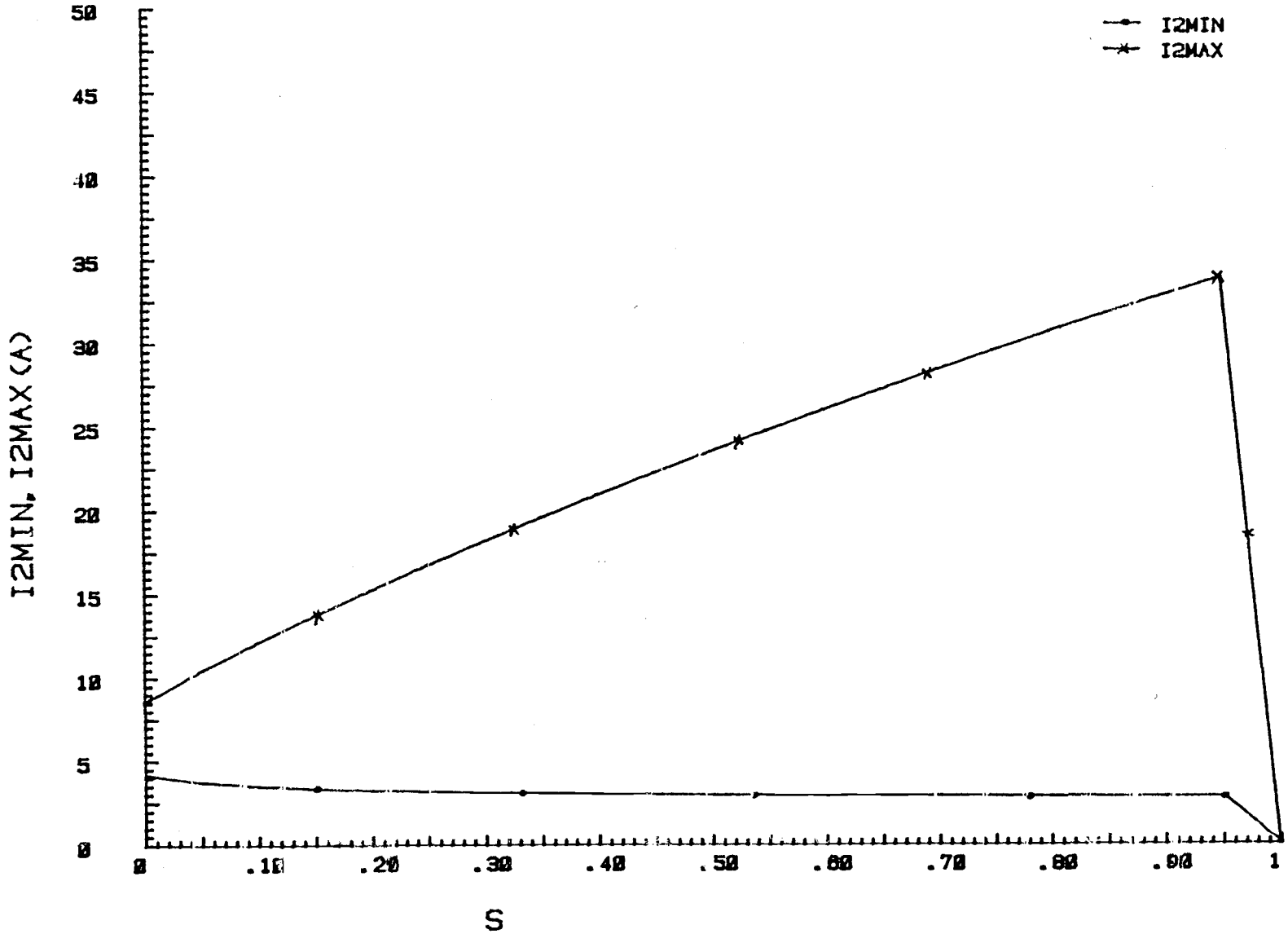

Fig.4.13 The curves of I_{2min} and I_{2max} versus slip s for input 4

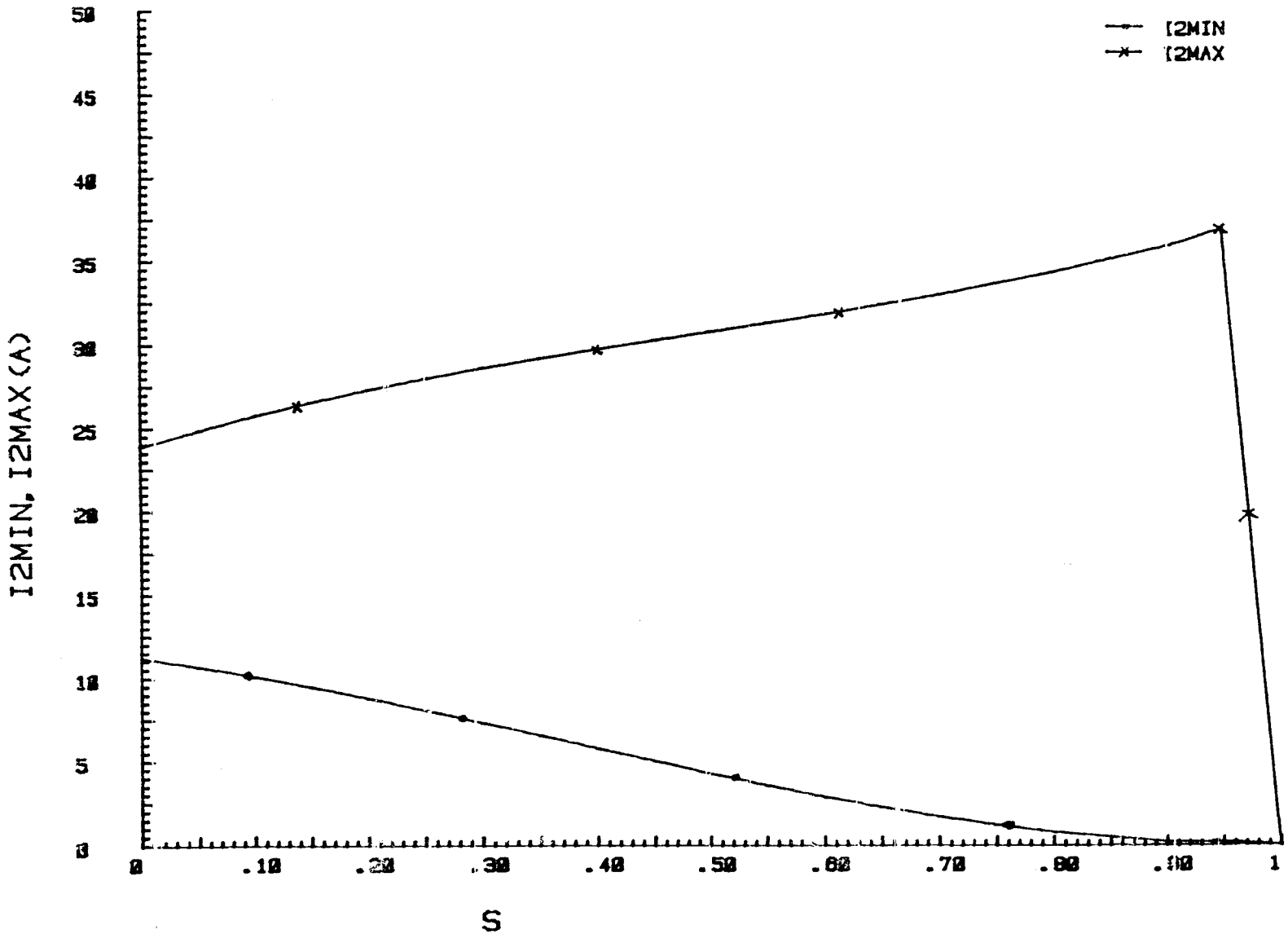

Fig.4.14 The plot of operating points I_{el} for input 1

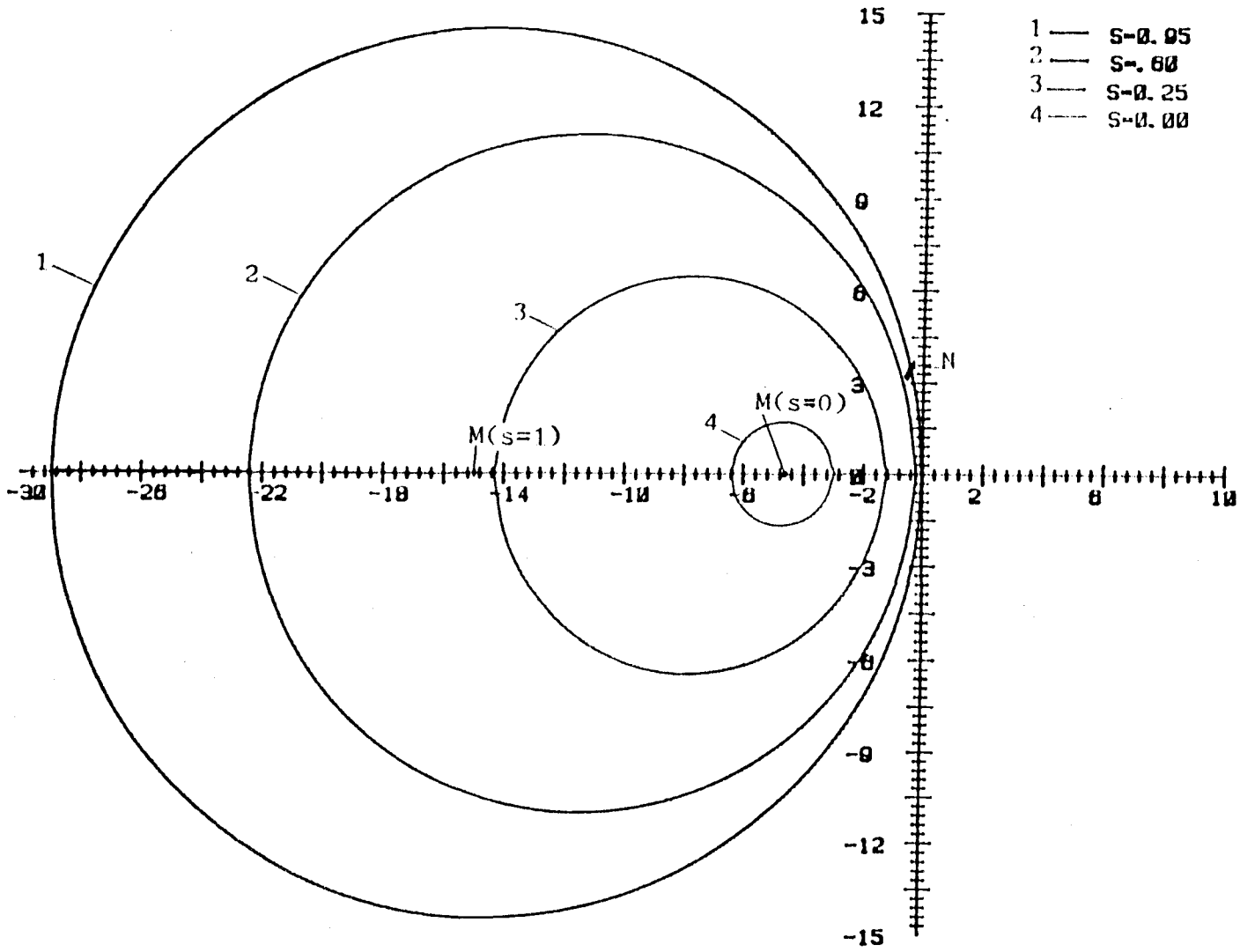

Fig.4.15 The plot of operating points I_{e1} for input 2

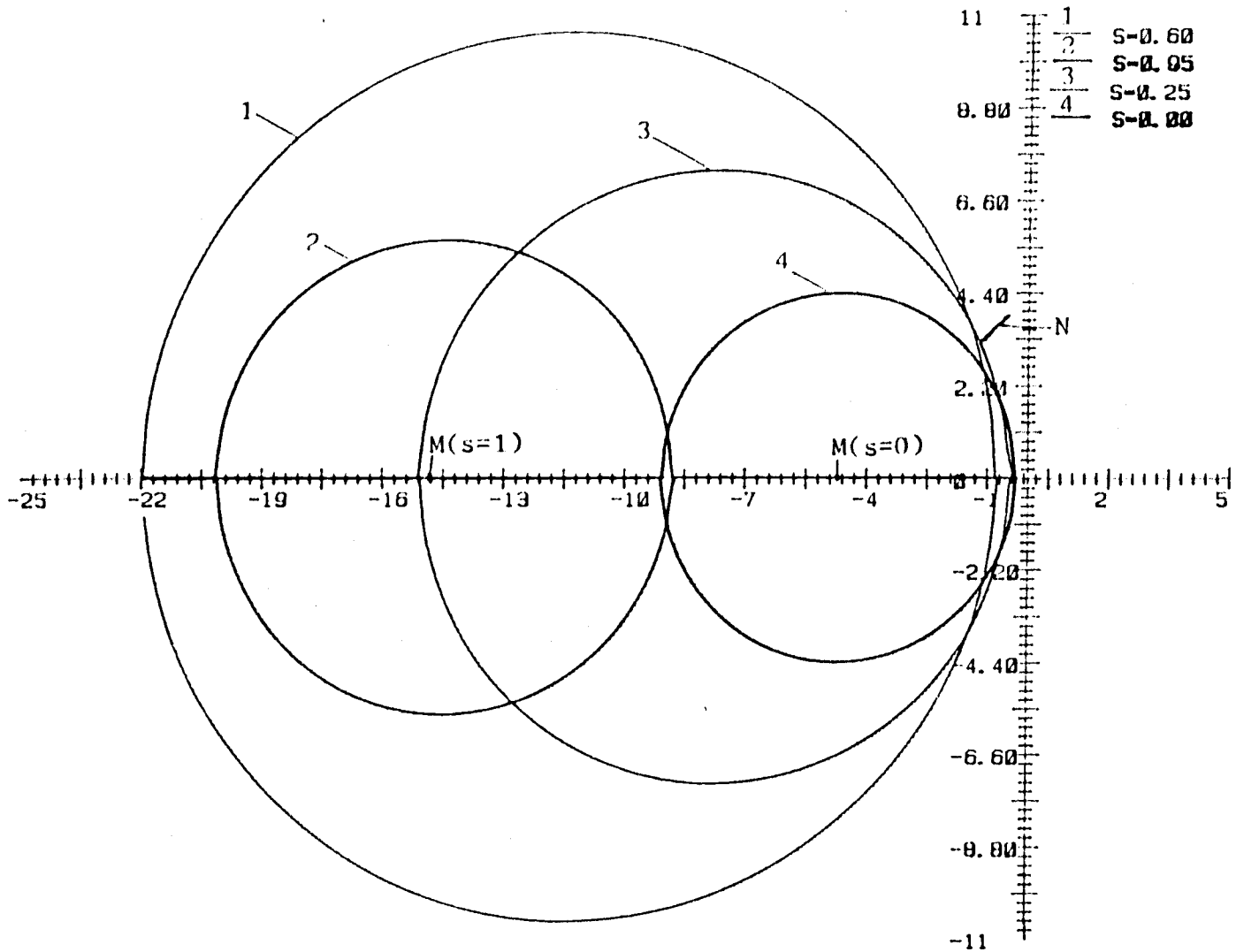

Fig.4.16 The plot of operating points I_{el} for input 3

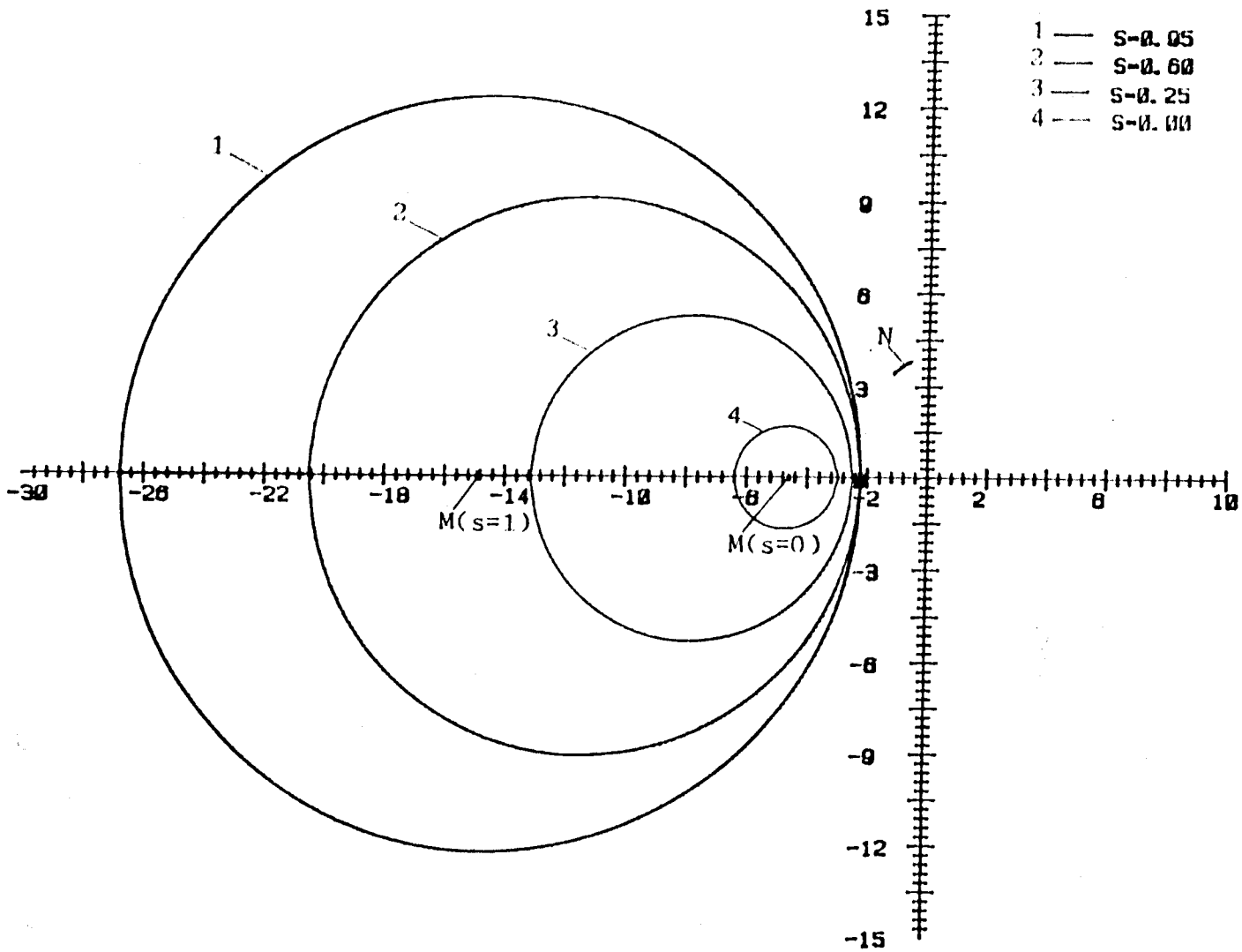

Fig.4.17 The plot of operating points I_{e1} for input 4

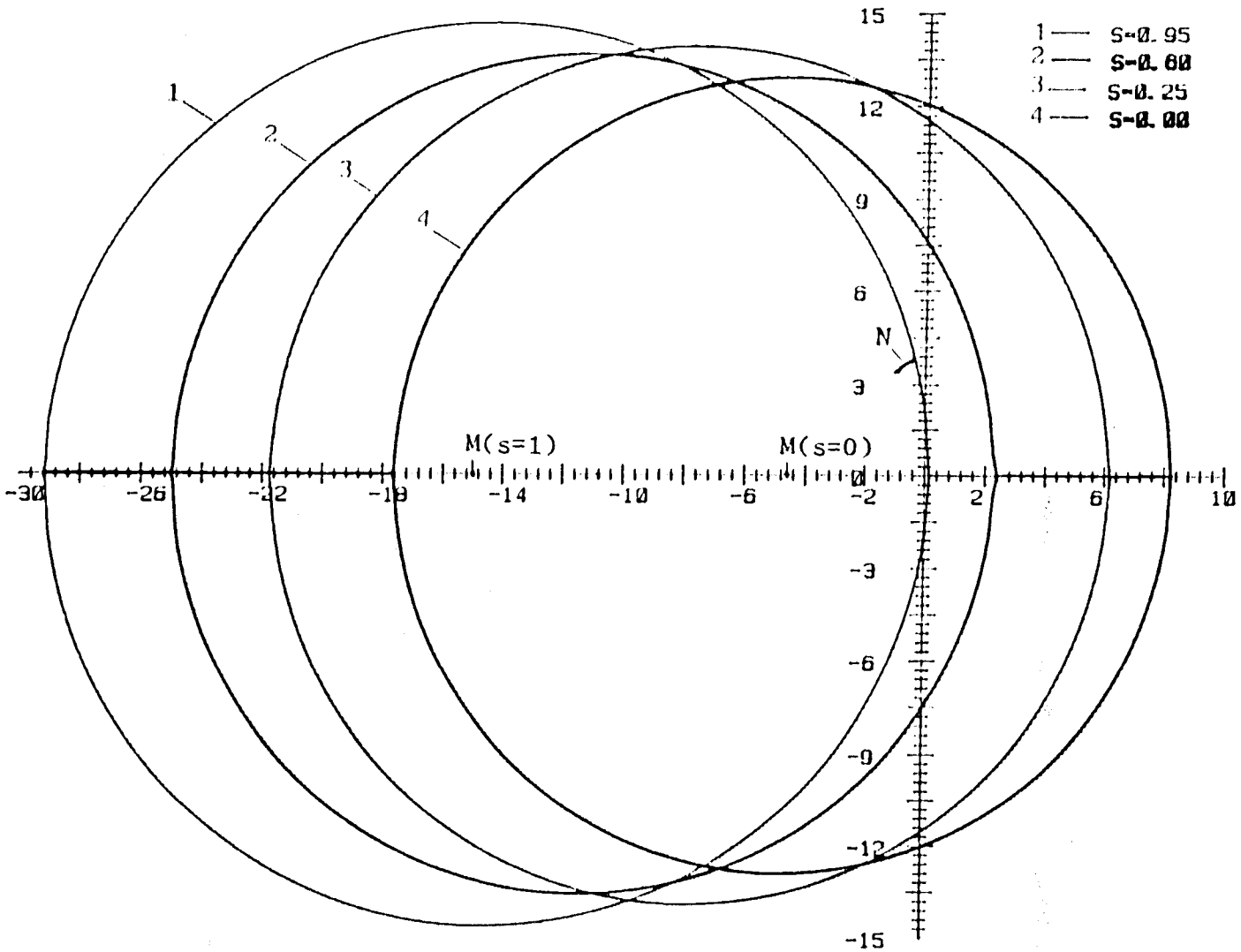

Fig.4.18 The plot of points N and M for different X_{m20}

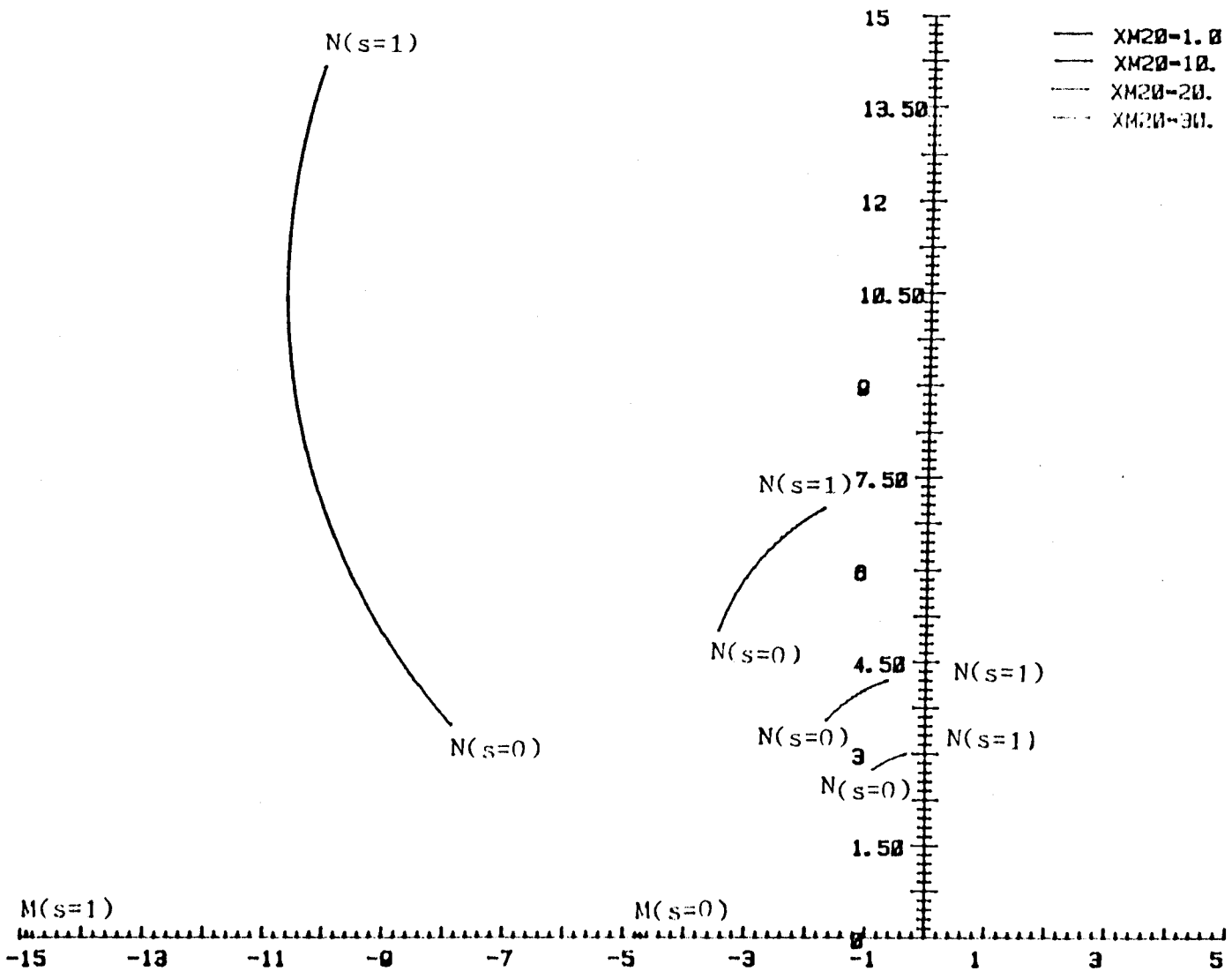

Fig.4.19 The curves of I_{2min} and I_{2max} versus X_{m20} for input1

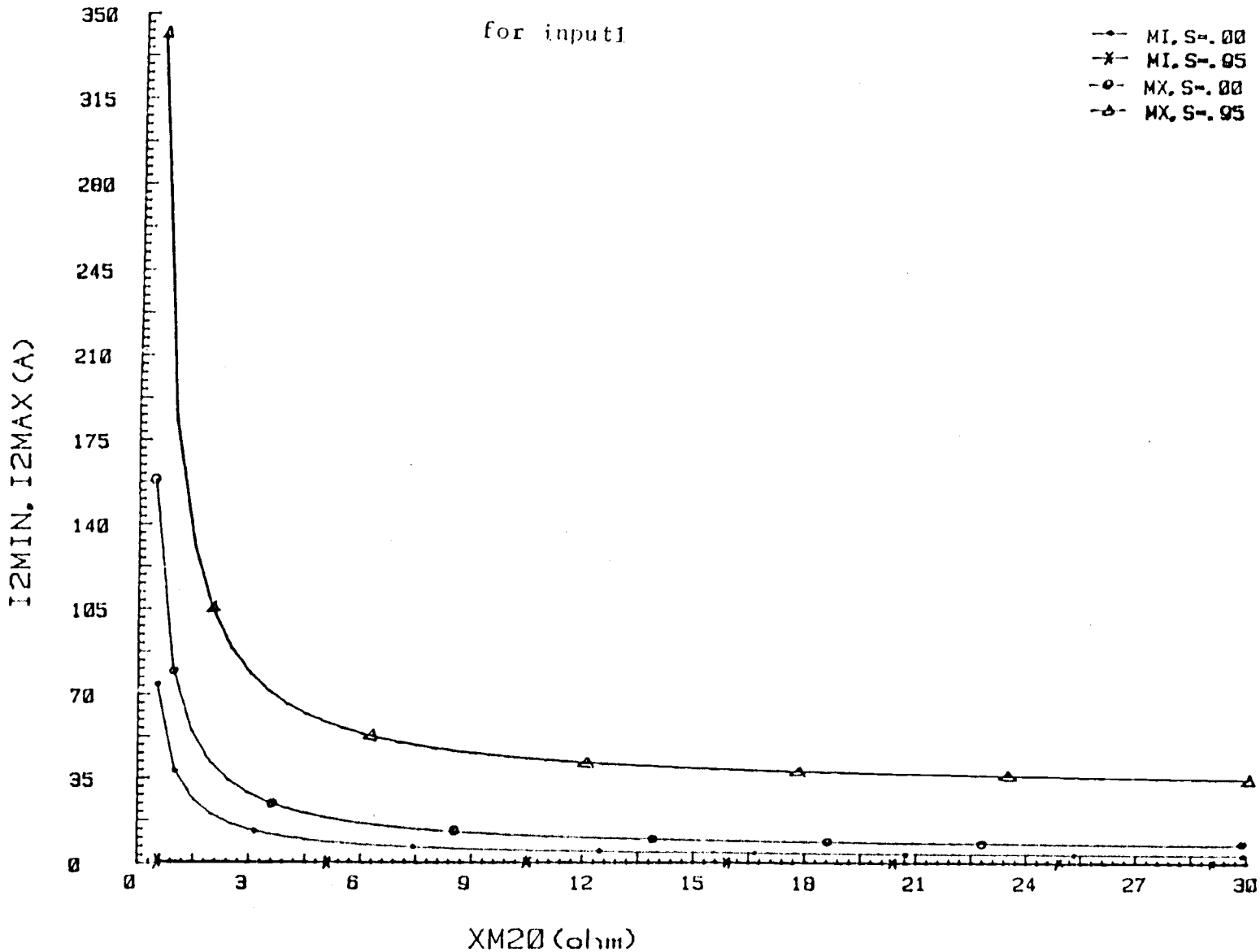

Fig.4.20 The curves of I_{2min} and I_{2max} for X_{m20}=1.0

for input1

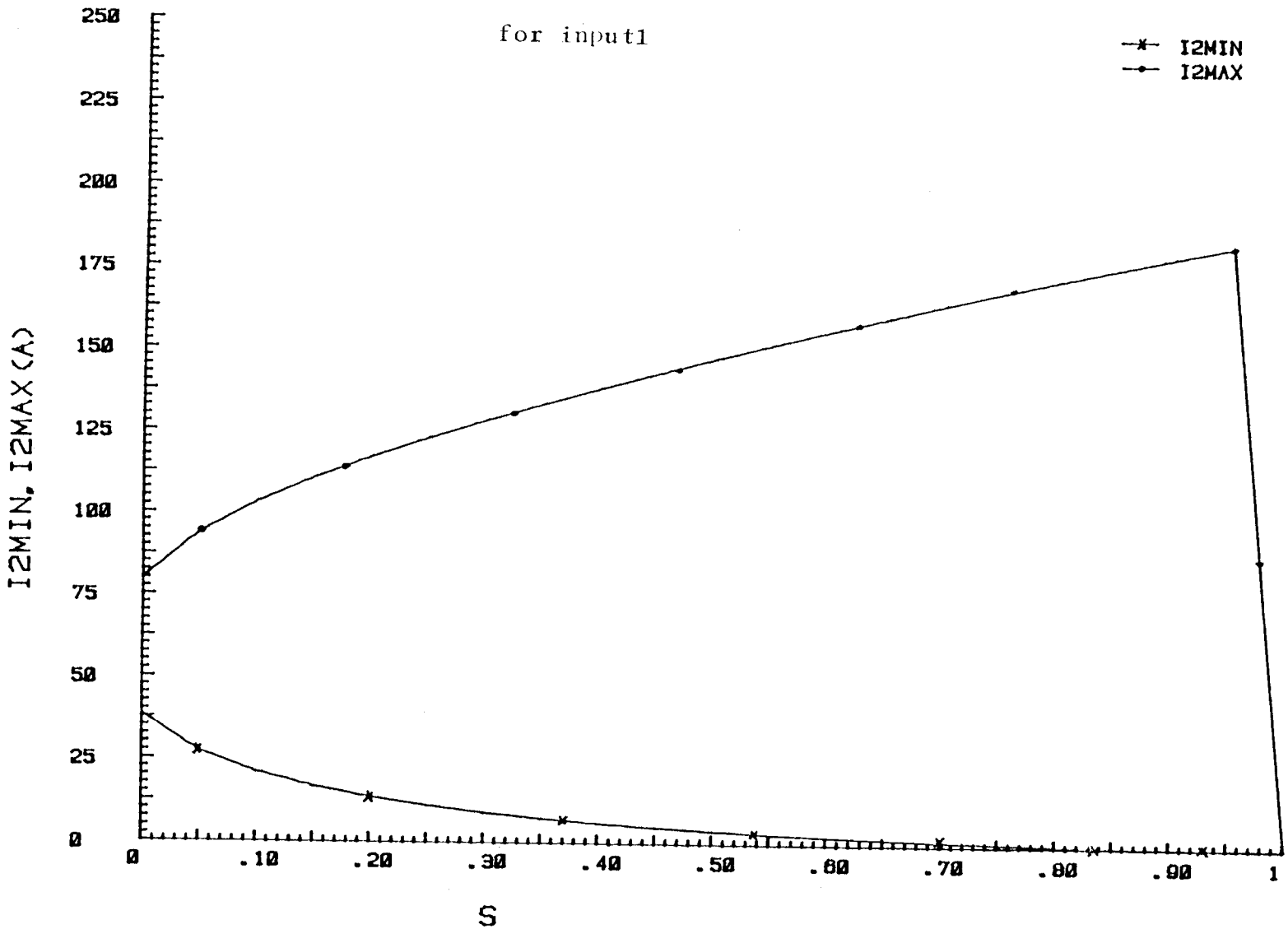

Fig.4.21 The curves of I_{2min} and I_{2max} for X_{m20}=10.0

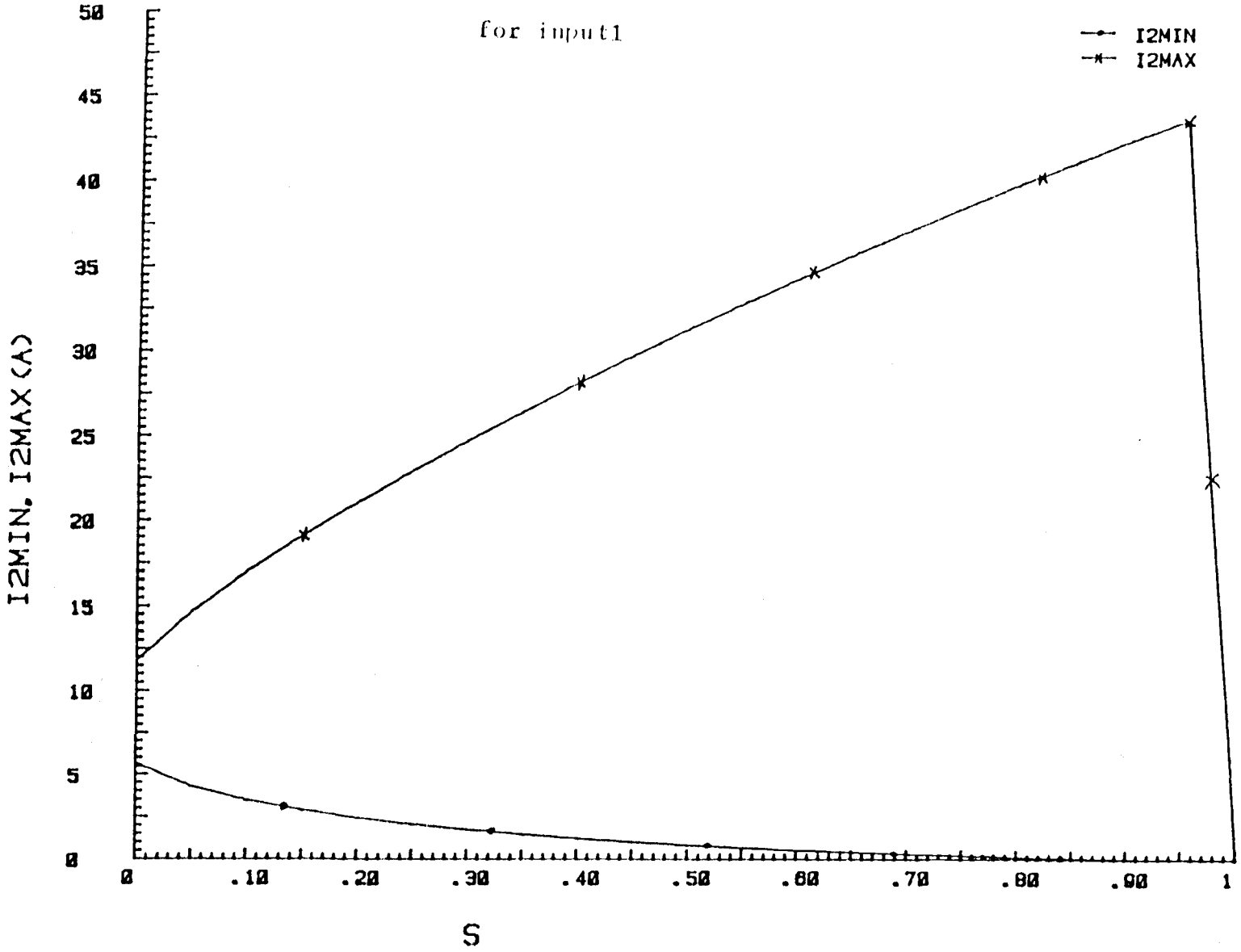

Fig.4.22 The curves of I_{2min} and I_{2max} for X_{m20}=30.0 for input1

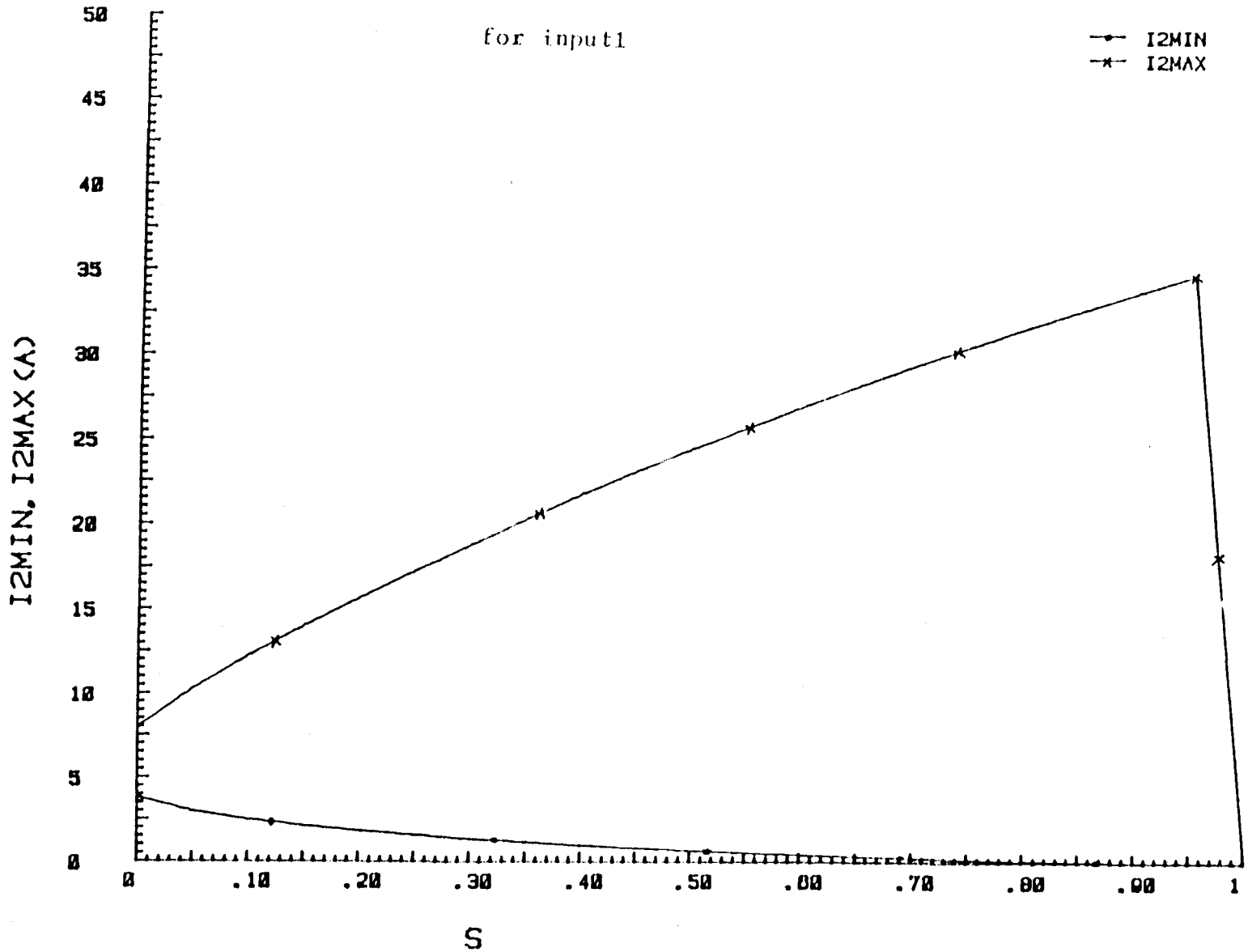

Fig.4.23 The curves of I_{2min} and I_{2max} versus R_{r1}

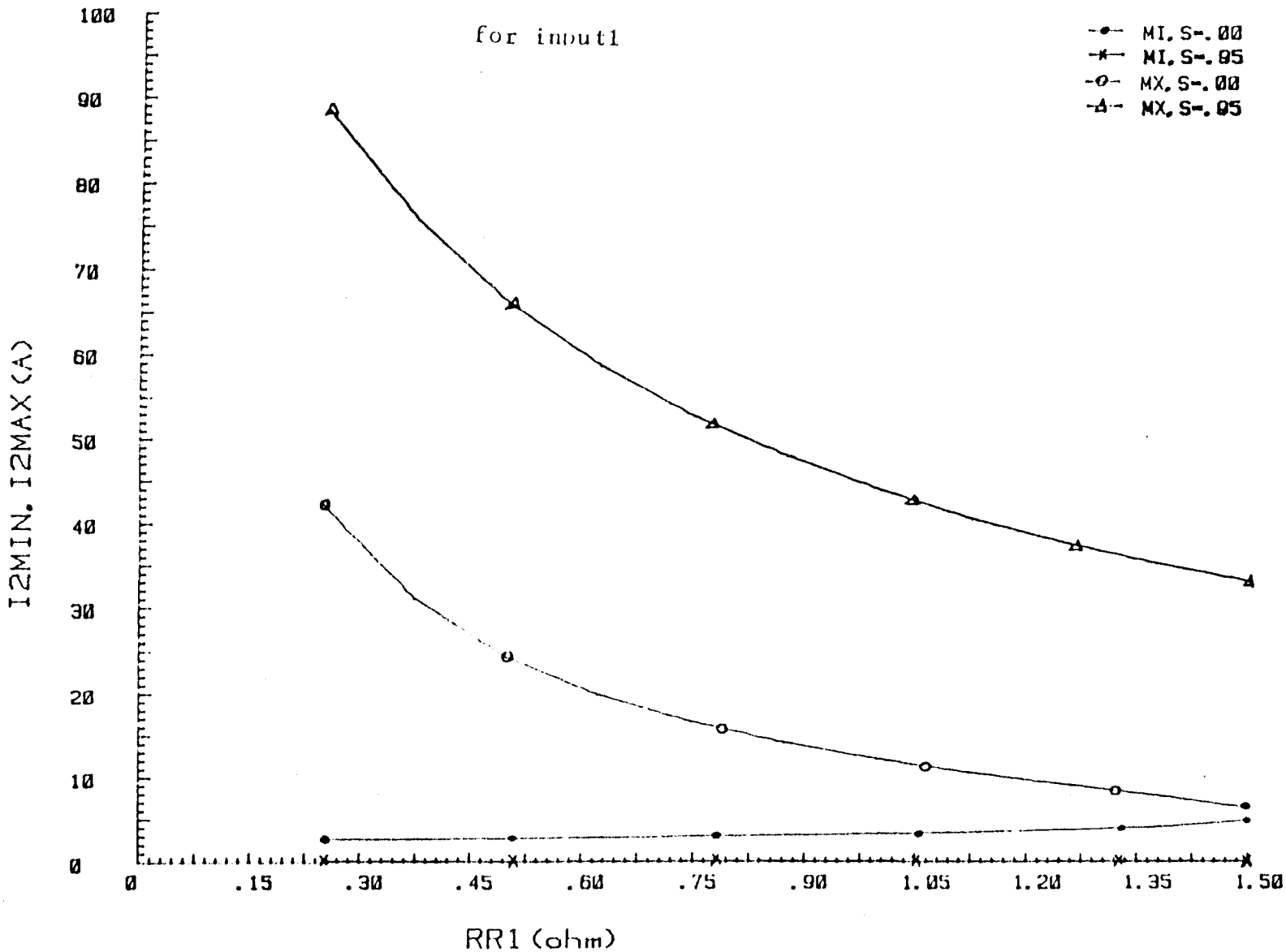

Fig.4.24 The plot of excitating current I_2 at Q=0

for input1

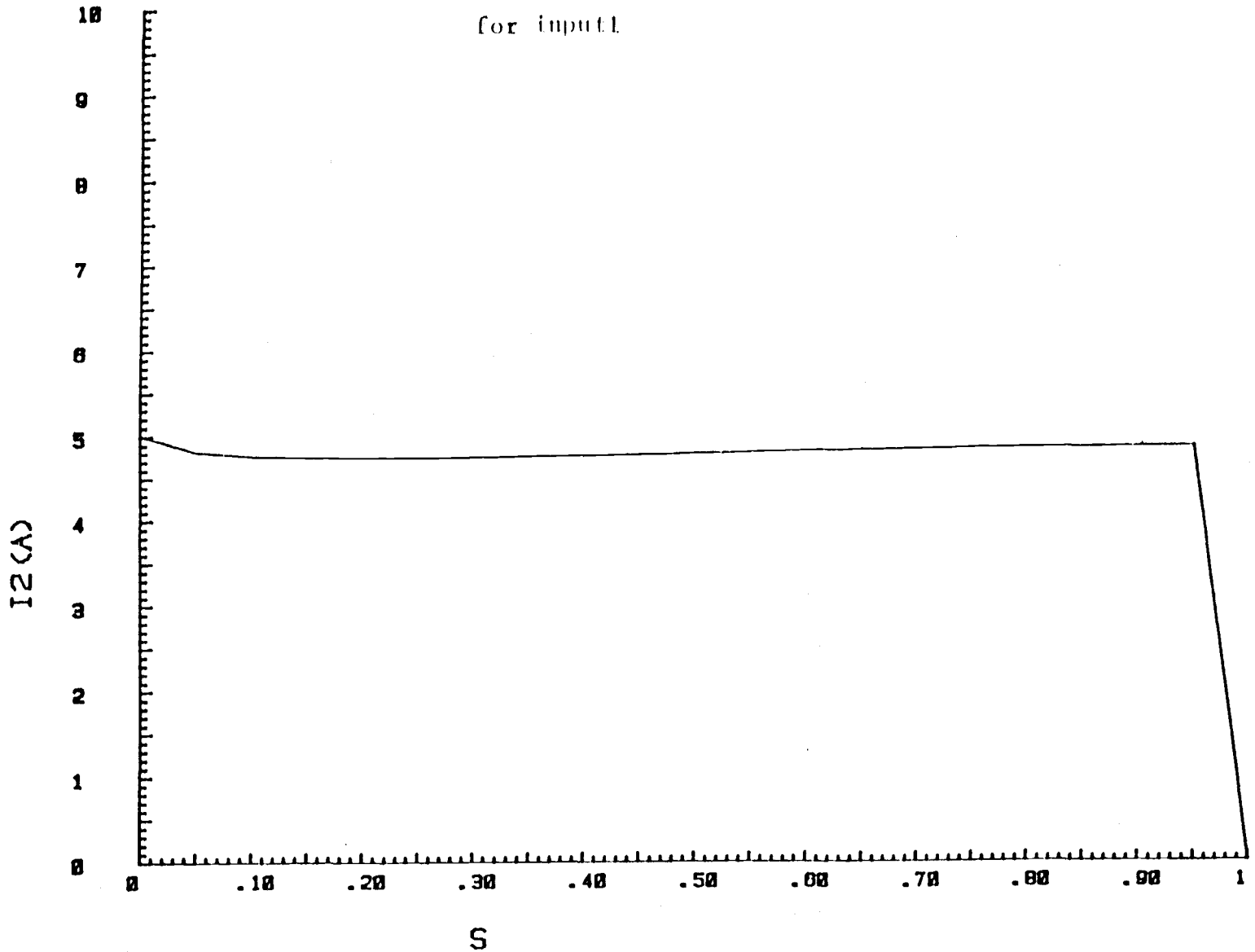

Fig.4.25 The plot of excitating current I_2 at Q=0 for input 2

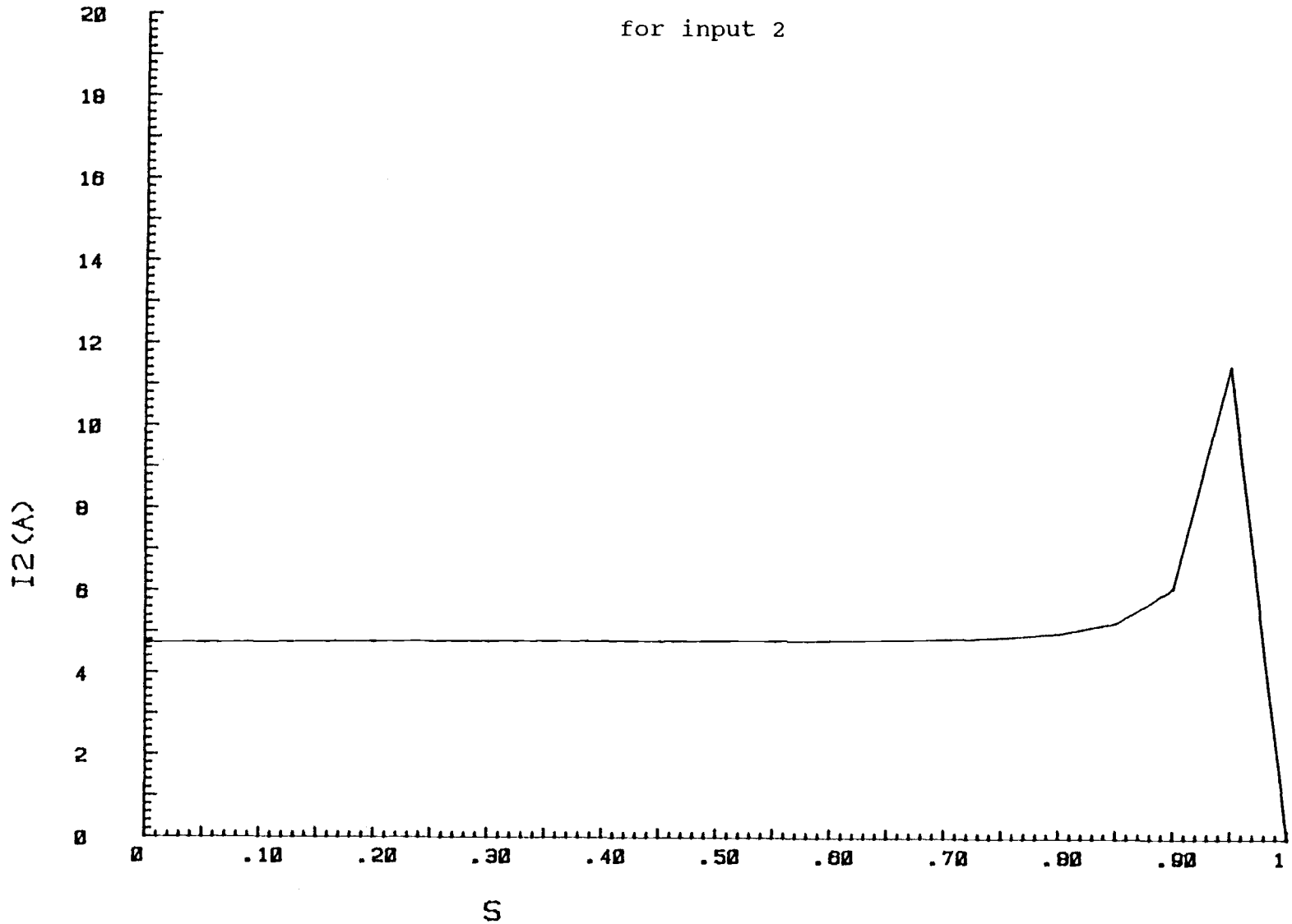

Fig.4.26 The plot of excitating current I_2 at Q=0 for input 3

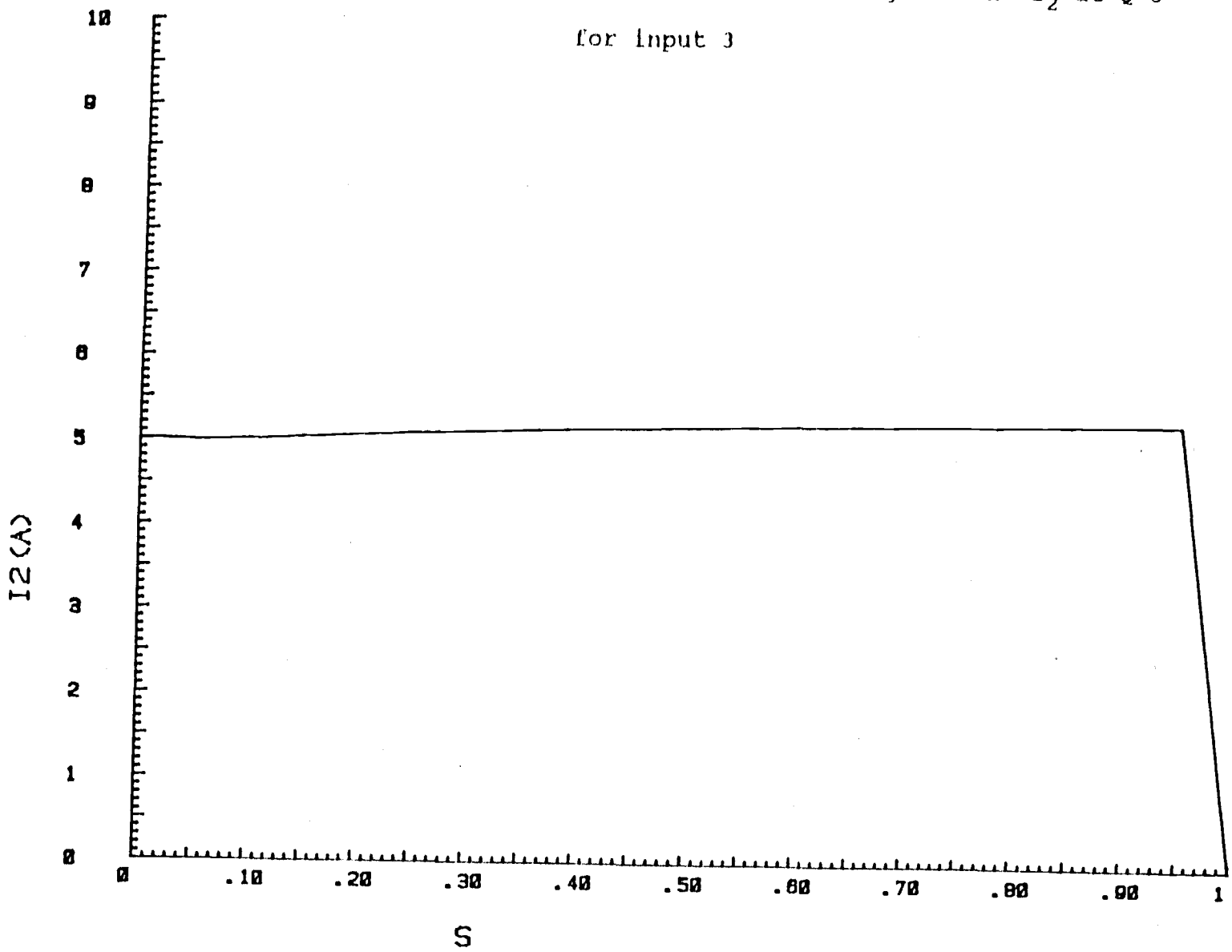

Fig.4.27 The plot of excitating current I_2 at Q=0 for input 4

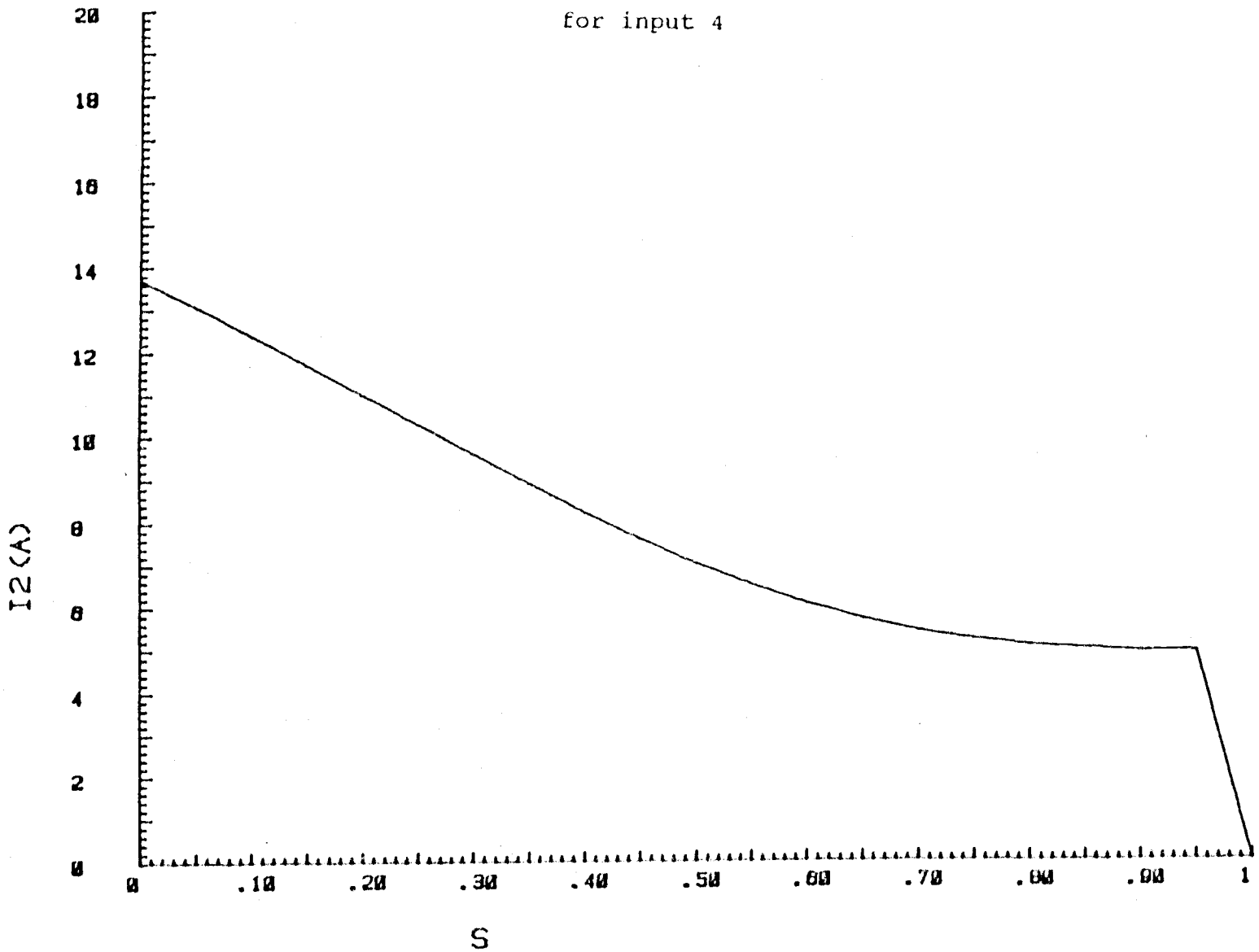

6. REFERENCES

[1] H.K.Lauw: " Characteristics of the doubly-fed machine in a hydro variable-speed generation system", Final Report prepared for U.S. Department of Energy Bonneville Power Administration, Contract No.79-85BP24332, June 1986 .

[2] A.R.W.Broadway, L.Burbridge: "Self-cascade machine: A low-speed motor or high-frequency brushless alternator", Proc. IEE Vol.117, 1970, pp.1277.

[3] P.N.Miljanic: "The through-pass inverter and its application to the speed control of wound rotor induction machines", IEEE Trans. on PAS, Vol.87, 1968, pp.234.

[4] M.Stöhr: "Vergleich zwischen stromrichtermotor und untersynchroner stromrichterkaskade", Elektrotechnik MaschBan 57, 1939, pp.581.

[5] W.Shepherd, A.Q.Khalil: "Capacitive compensation of thyristor-controlled slip-energy-recovery system", Proc. IEE Vol.117, No.5,1970, pp.948.

[6] A.Kusko, C.B.Somuah: "Speed control of a single-frame cascade induction motor with slip-power pump

back", IEEE Trans. on Industry Application, Vol. 14, No.2, 1978, pp.97.

[7] C.D.Cook, B.H.Smith: "Stability and stabilisation of doubly-fed single-frame cascade induction machines", Proc. IEE Vol. 126. No.11, 1979, pp.1168.

[8] M.M.Liwschitz: "Damping and Synchronizing Torque of the Doubly-Fed Asynchronous Machine," AIEE Transactions, Vol.60, 1941, pp.923.

[9] J.C.Prescott, B.P.Raju: "The Inherent Instability of Induction Motor Under Conditions of Double Supply," Proc. IEE, Vol.105, (C), pp.319, 1958.

[10] H.K.Lauw, J.B.Klaassens, N.G.Butler, D.B.Seely: "Variable-Speed Generation with the Series-Resonant Converter," IEEE Trans. on Energy Conversion, also presented at IEEE PES Winter Meeting, Jan. 1988, New York.

[11] W.B.Gish, J.R.Schurz, B.Milano, F.R.Schleif: "An Adjustable Speed Synchronous Machine for Hydroelectric Power Applications," IEEE Trans. on PAS, Vol. PAS-100, May 1981, pp.2171.